Density, Porosity & Constituent Fractions in C-C Composites, Ceramic Composites, Hybrid C-C/CMC Composites and Carbon Cloth Phenolic Ablatives

Randy Lee *Marshall Space Flight Center* *June 2009*

INTRODUCTION AND DISCUSSION

'Real' densities for constituents of the carbon-carbon/silicon carbide (C-C/SiC) material used in the launch abort motor system are given in Table 2 on page 8, immediately followed by sources and justifications for these values. Then, porosity data for the carbon cloth phenolic (CCP) ablative material used in the RSRM nozzle skirt is examined on page 26 in an analogous fashion, but first, a few background definitions are in order. In contrast to 'bulk' density, real density is supposed to represent the impervious density, sometimes referred to (confusingly) as the true density, perhaps more appropriately as the apparent density or skeletal density (and often misinterpreted as the 'specific gravity') . . . In fact, *true density is the bulk density with the porosity fraction factored out*. All three properties, bulk density, skeletal density and porosity are generally acquired in a single test using one of the Archimedes-type 'buoyancy' (liquid displacement) techniques which calls for three weight measurements on each material sample: the dry weight, the suspended weight (as it is buoyed in the test fluid) and the saturated weight (which requires expert handling techniques for precise determination). In lieu of the saturated weight, it is sometimes possible to obtain the bulk volume of the sample geometrically or by other means, giving sort of a hybrid test approach.

In any case, the actual results acquired from all of these methods is highly dependent on the specific intrusion technique applied and the particular liquid used (how it interacts with the substrate). To fully occupy the available (open) porosity of a material, the fluid must 'wet-out' the pore surfaces and then overcome the capillary forces in order to displace the air inside the pores. For coatings and thin materials, simple immersion or passive soaking of the substrate in the test liquid is often adequate. However, in order to ensure effective penetration of the porosity in most materials, the fluid must be forcefully intruded or impregnated into the pore network under the actions of vacuum and pressure, or by boiling the liquid with the test samples in it. The latter approach is based on the ASTM C-20 water-boil test, while the former is reflective of an original technique developed independently several years back (both procedures have been optimized and personally conducted over 2000 times on a variety of composite materials, their constituents, various monoliths, metals and other nonmetallics).

Absolute values for these properties are difficult to acquire. Complicating this is the fact that essentially *all composite materials contain a certain fraction of 'closed' porosity* which is not interconnected and is impenetrable to intruding fluids (even with vacuum and pressure application). The *total porosity* is equal to the sum of the open and closed porosity fractions and can consist of any combination of holes, pores, tunnels, channels, dendrites, voids, cavities, bubbles, inclusions, cracks and delaminations. Depending on the degree of pore network interconnectivity, fluids over a wide viscosity range will permeate a material's macro-porosity (those with critical passage diameters or dimensions > 50 nm) and much of its meso-porosity (2 nm < d < 50 nm), while leaving its micro-porosity (d < 2 nm) completely unviolated.

Table 1. Established porosity size categories giving examples of relative composite component sizes for comparison.

Microporosity < 2 nm	**Mesoporosity** 2 nm – 50 nm	**Macroporosity** 50 nm – 100 nm	**Metaporosity** > 100 nm	**Ultraporosity** > μ
water, solvents, unreacted crosslinkers, monomers, dimers, trimers, tetramers, straight chain non-branched oligomers and small linear polymers . . . but not necessarily their agglomerates	moderately branched high molecular weight polymers, folded high tertiary structure polymers, small adducts and some of their agglomerates	branched prepolymers, larger resin polymers and their conglomerates, small crosslinked segments and fragments, very low aspect nanoparticles may pass into pore openings before lodging	most particle fillers and moderate aspect nanoparticles, especially their agglomerates may pass into pore channels but will likely clog passages up to a micron and greater	voids, large pores, micro-cracks and pore clusters not driven by volatiles may represent dry areas with low resin content; primary spaces where particles and their agglomerates come to rest

Without a doubt, *density and porosity values are purely a function of the technique used to measure them* [1]. Since all three properties are integrally related to each other, corresponding values for the bulk density ρ_b and true density ρ_t are a natural consequence of just about any method used to determine the 'open' or 'apparent' porosity p_o of a material that can be defined by[2] . . . $\rho_b = (1 - p_o)\rho_t$. This is substantiated by the observation that bulk and true densities are indistinguishable for so-called non-porous materials such as float glass and many metals.

Handbook values for crystal densities are often obtained via x-ray diffraction methods (XRD) and tend to represent the *absolute density* of a material (sometimes called the 'x-ray density'). Of course, XRD is most appropriate for indicating lattice parameters in crystalline (Bragg) materials, but x-ray *scattering* techniques can reveal porosity-related features inherent within non-crystalline structures. Helium pycnometry is another method for determining apparent density and porosity, and is it applicable to many solid materials, porous, non-porous, amorphous or crystalline. For porous materials, pycnometry is capable of deriving skeletal volumes by infiltrating much of the total porosity with angstrom-sized He atoms and reconciling the measured pressure change through the Ideal Gas Law. Of course, porosity infiltration via Darcy flow is the intended mechanism here, not diffusion or absorption (Fickian diffusion may sometimes be a potential concern with pycnometry techniques).

A separate measurement for the dry weight allows one to estimate the true (near absolute) density for the material, sometimes called the 'helium density'. Also, with a separate measurement for the bulk volume (such as that obtained by geometrical dimensioning or laser techniques), this hybrid test method can often provide results very close to the theoretical limits for the total porosity, the bulk density and the true density of a material sample in which the porosity is *interconnected*, at least through micro-channels [3]. Thus, the fraction of 'available' or 'open' porosity now becomes a conditional and subjective quantity. From an application perspective, the bulk density and associated porosity are a function of the processes used to manufacture the material, while the true density may be the only 'absolute'. In essence, the concepts of open porosity, closed porosity and interconnectivity are all established exclusively by the manufacturing processes applied, the constituent materials incorporated and the characterization techniques used to define the material.

[1] Porosity characteristics of the various composites and their phases are discussed starting with the section "Open (Liquid-Permeable) Porosity: Functional Characterization & Estimations" which will be cover later in the in the report..

[2] Reference formula 4A in Appendix A at the end of the report. Consult Appendix A for explanations of these formulas and the subscript notation used throughout.

[3] The section, "True Densities: Survey and Comparison" on page 27 contains an excellent summary highlighting the various levels of densities in porous materials.

On the topic of porosity characterization, another aspect which should be taken into account during test measurements is related to the effects of extraction and machining during sampling and specimen preparation. For 2-D laminated systems, porosity and permeability are highly anisotropic properties incorporated into the composite during the manufacturing process, while certain 3-D composite systems may be slightly more isotropic. In any case, permeability and pore/void accessibility will vary from one face of the test sample to the next. This is easily verified with 2-D laminates when comparing through-the-thickness permeabilies to cross-sectional measurements in-plane (parallel to the laminate direction). Undoubtedly, machining and sample sectioning open up pores and cavities which may have otherwise been considered as part of the closed porosity fraction. Thus, unless the machined edges are intentionally sealed over, typical density/porosity test results will reflect a net open porosity which is a combination of accessible pores across the primary surfaces and closed pores/voids opened up or exposed by the sample sectioning process.

Closed voids, micro-porosity and interconnectivity are subtle properties that are often overlooked and difficult to quantify, but there is ample historical evidence showing that their effects are tied to a host of anomalies and failures . . . they should not be disregarded. For many material systems, such as multiple interface composite materials, most of the macro- and meso-pores, voids and channels are accessible to both fluids and gases, while the majority of the porosity/void fraction that appears to be impervious to intruding fluids is actually interconnected via micro-channels (which of course can only be seen under SEM magnification). Micro-porosity channels can provide access into the closed pore volumes (or much of it) as they may be permeable to gases, particularly He atoms. However, within certain monolithic constituents, these closed regions become completely isolated and hermetically sealed from penetrating liquids and gases during the thermal forming process.

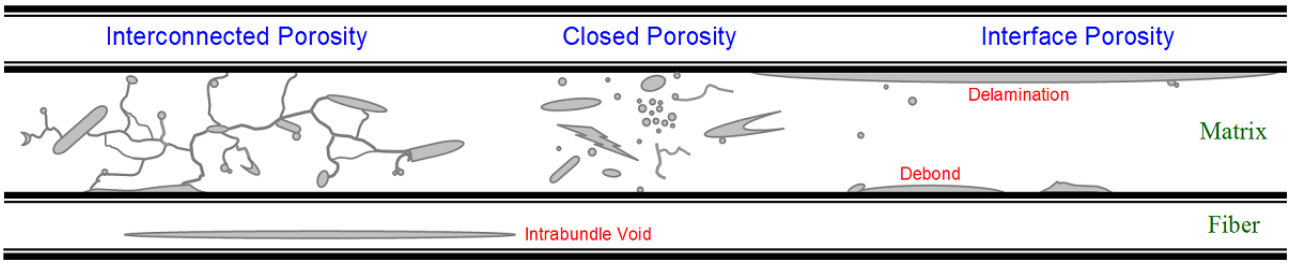

Figure 1[1]. Graphical display of possible pores generated during a pyrolysis of crosslinked polymer thermosets. Note: The author has experimentally conducted over 1000 tests estimating open porosity values on samples of polymer matrix composites, 3-D composite samples, cured matrix resins, glassy carbon, ceramics and various carbon-carbon forms via water impregnation, mercury porosimeter, helium psychometry, and also developed an original test method for measuring open porosity of samples down to about 0.3nm size.

Materials of interest in this category include glasses, glassy carbons and glassy ceramics, in particular, carbonized organic polymer thermosets, such as charred phenolic resin[2], and low temperature pyrolyzed pre-ceramic polymer thermosets, such as Starfire's SMP-10 carbosilane resin, as well as the silazanes (ex. KDT Ceraset) and siloxanes (ex. Blackglas). Uniquely, hermetic inclusions, voids and bubbles develop in these amorphous monoliths during the thermal forming or conversion process and many of these may contain trapped volatiles which have no way of getting out of the system during subsequent thermal excursions, other than to rupture the enclosing matrix walls when their pressures exceed the tensile strength of the matrix. In other situations, there may be micro-channels interconnecting these closed volumes but the rate of pressure increase during excursions

[1] All technical descriptions and illustrations in this paper are the interpretation and handiwork of the author except where noted.

[2] "Small-Angle X-Ray Scattering from Glassy Carbon", W. S. Rothwell, J. Appl. Phys. 39, 1840 (1968)

exceeds the physical capability of the pore network to effectively facilitate the rapid gas out-flow from the system.

From a practical perspective, bulk density characterizations via any of the Archimedes test methods are most appropriate for composite material systems in which the matrix is generated from liquid precursors, such as polymer solutions and resins. This would encompass all continuous reinforcement and chopped fiber systems, particulate composites, adhesives, plastics and coatings (including GRP, GCP, SCP, CCP, C-C/SiC, RCC, carbon/epoxy, polyimide/BMI systems, EA-9394, TIGA-901, and so on...). Similarly, open porosity is most appropriately defined by the volume fraction that is available to liquid matrix precursors, polymer solutions, resins and test fluids. This portion of the total porosity would pertain to most of the macro-pores and some of the meso-pores. The closed porosity might be hermetically sealed to gases or, some of it may be interconnected to other voids via micro-channels. In any case, during curing operations, pyrolysis and firing cycles, these definitions will waver because pore dimensions generally increase with temperature allowing the pore channels to accommodate boiling monomers, dimers and reaction volatiles in larger quantities and molecular sizes. Herein lies a potential benefit for the supplemental use of gaseous pycnometry methods.

Mercury porosimetry, which produces impressive data tables, charts and graphs depicting pore diameters, dimensions and surface areas, is known to physically damage these types of materials by crushing the internal pore structure and generating erroneous results. These conclusions have been demonstrated through extensive independent testing and substantiated by other workers within the field. The contact angle of liquid mercury on carbon/ceramic surfaces is highly acute (that is, Hg is very non-wetting). Under standard intrusion pressures of 30,000-60,000 psi, it is not difficult to visualize how this very heavy liquid can bludgeon its way through pore walls degrading the very property it is suppose to measure. While a few workers still report results from this technique even today, caution should be exercised when interpreting results produced by Hg porosimetry.

Porosity in composite materials is often treated as a volumetric fraction *within the matrix phase*. This may not seem entirely realistic at first glance. After all, pore walls and surfaces actually include a mixture of matrix and fiber surface contributions which underscores the practical differentiation between ‘composite porosity’ and ‘matrix porosity’. Additionally, constituent fiber bundle tow and rovings as well as the individual fiber filaments themselves typically contain their own network of pores and micro-voids, some of it open, but much of it closed and impervious. However, from a conceptual perspective, both open and closed porosity can be envisioned as an entrained volume fraction housed within the matrix phase by virtue of the fundamental relationships which define the primary constituent fractions, such as the composite bulk density expressed in terms of the fiber/matrix volume fractions and respective densities, namely . . . $\rho_b = f_v\rho_f + m_v\rho_m$. It is apparent from this classical expression [1] that the porosity fraction cannot be part of the raw fiber volume v_f , so it must functionally be included within the ‘net’ matrix volume v_m . In actuality, the porosity is indeed a separate volume fraction, but since it has no density, it is necessarily housed within one or more of the constituent volume fractions. Moreover, during composite densification operations, the matrix volume increases at the expense of the porosity while the fiber volume remains constant [2].

[1] Reference formula 1A in Appendix A at the end of the report. Consult Appendix A for explanations of these formulas and the subscript notation used throughout.
[2] Composites whose volumes are infinitesimally constant throughout densification will be further considered later in the report..

Large voids and cavities are often localized along fiber bundle intersections. Some are interconnected with the regional porosity, others are impervious. Additionally, when cured properly, matrix systems that release solvents, reaction volatiles, condensation products, monomers, dimers, trimers, etc... will tend to create an extensive, branched network of interconnected micro-channels leading from the core of the composite body to the outside. This includes the phenolics, many polyesters, polyimides, di-functional silanes and silicones (all of which release condensation water and/or methanol, monomers and dimers), and of course, the pre-ceramic carbosilanes and silazanes (even though these cure/crosslink via free radical addition, silane-bound active hydrogens are readily expelled throughout their pre-ceramic history, along with lesser amounts of silane and small aliphatics). Most (modern) epoxies and urethanes also cure by addition (rather than condensation) . . . but there are no supplemental volatile releases accompanying the formation of epoxy amine links or urethane linkages, which means these cured systems contain little micro-porosity (while molecular moisture will readily diffuse through epoxy mediums, Darcy flow is essentially nonexistent).

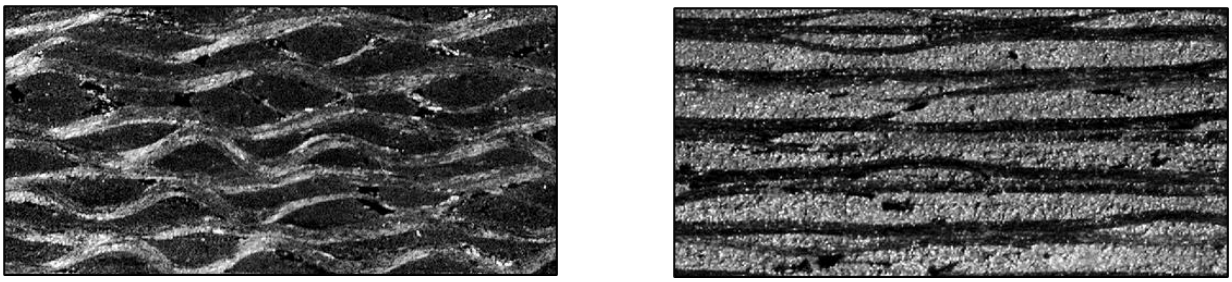

Figure 2. Left: 20X cross sectional view of carbonized rayon fabric in carbonized furfuryl alcohol resin matrix (Reinforced Carbon-Carbon, RCC). Right: 20X cross sectional view of carbonized PAN fabric in carbonized phenolic matrix (Advanced Carbon-Carbon, ACC). Not all the porosity can be seen in these micrographs. The rayon sample indicates larger pores near or along fiber-matrix interfaces while the PAN sample may indicate pores along the fiber-matrix interfaces and within the fiber bundles themselves. Images by Randy Lee, 1986.

A much better cross sectional view of the RCC material conducted via SEM analysis is given in Figure 3 taken during some of the evaluations conducted at NASA Langley Research Center during the last few missions of the Space Transportation System (STS) on the Shuttle's carbon-carbon leading edge panels. Several analyses were conducted and reports issued by the author during that time period including "RCC, Evaluation of Defects and Failures for the STS-120 Mission", "RCC, Evaluation of Defects and Failures in Shuttle Leading Edge Joggle Regions, Report 1" and "RCC, Evaluation of Defects and Failures in Shuttle Leading Edge Joggle Regions, Report 2, Randy Lee.

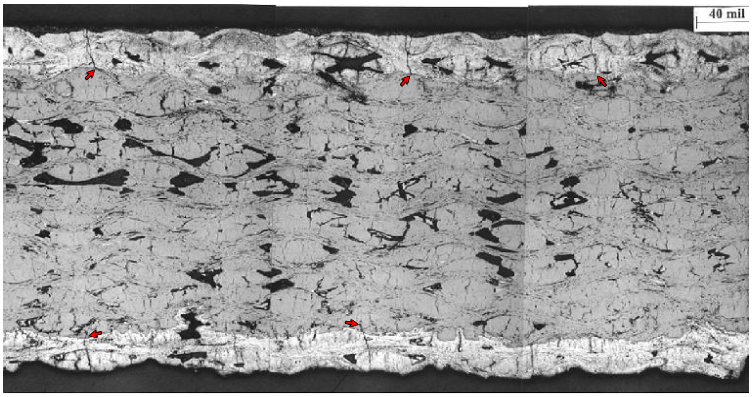

Figure 3. "STS-120 Flight Readiness Review" presented on October 16, 2007 by Ralph Roe

Figure 3 shows a small portion of one of the cross sectioned RCC panels conducted prior to the STS-120 mission for evaluation. As mentioned previously, the substrate consists of carbonized rayon fabric reinforcement within a carbonized furfuryl alcohol matrix. However, after the densification phase is complete, a 3000°F SiC ceramic conversion coating is applied on the outer surfaces of the substrate panel for oxidation protection (top and bottom in the image). This was the finished stage of the RCC panels before deployment. Porosity can be seen in both the C-C substrate and the SiC phase. Since the substrate pores apparently were not filled during subsequent resin impregnation/pyrolysis densification cycles, at least some of them could be considered as 'closed porosity'. Porosity in the SiC gradient conversion coating phase was formed during the coating process. Porosity is typically generated during processing due to outgassing and volatile release associated with the various time-temperature heating profiles that are applied throughout. Again, some of this porosity may be interconnected while some of the voids and pore channels may completely closed off. The only supposition one can draw is that all the pores seen in the image are 'open' relative to the cross sectioned surface.

Now when escaping molecules encounter hard objects, such as fibers and particle surfaces, the path begins to intertwine as it crosses other escape paths ultimately resulting in a highly interconnected, dendritic pore structure that is open and permeable throughout. While there is certainly a downside to porous matrices, this interconnectivity provides the composite structure with a unique mechanism for stress relief and volatile release while enhancing toughness factors (fracture control). Additionally, it imparts unique ablative properties to the system by facilitating the early removal of pyrolysis volatiles during charring and burning processes, and it opens the door to an array of unique post-fabrication techniques such as densification, gradient phase conversion and diffusion bonding.

It is surmised that the density/porosity values indicated by the subcontractor, XYZ (a producer of the *n*-D material components considered for the ARES Launch motor) for their C-C/SiC material were obtained using buoyancy techniques, possibly one of the many ASTM methods readily available or perhaps a modified version thereof. It must be realized however, that density/porosity values obtained from these types of techniques should be considered as 'relative', and thus it follows that all the other parameters and properties subsequently derived from these measurements, are also relative. This would include estimated fiber volumes, resin contents, matrix volumes, residual volatiles and char yields, as well as certain constituent densities and any other fractional quantity that is estimated from measured values of density or porosity. These are subtle aspects one should keep in mind every time a data table is presented containing values for density, porosity or matrix/resin content.

Three dimensional and multi-dimensional weaves or 'preforms' (3-D and *n*-D) comprised of carbon fibers is complex and presents a slightly different concept of composite materials in terms of their porosities. Instead of providing the major strength axes in one or two dimensions, multiple dimensions of reinforcement support are established and these systems are generally more complicated to produce. Since their inception in the 1980s, it has been well established that pseudo-isotropic *n*-D composites usually cannot replace 2-D anisotropic laminated composites in most high strength

applications, but at least they provide significant mechanical properties in more than two dimensions as with laminated composites which are often needed for many requirements that laminated composites cannot provide.

Configurations provided by XYZ, as with most *n*-D producers, composite reinforcements start out as dry woven billets consisting of fiber bundles in multiple directions which were then lightly rigidized impregnating a small amount of resin into the dry structure and cured prior to the densification stage. The stiffen reinforcements comprised of multi-dimensional preform PAN carbon fiber weaves can then be matrix-densified via organic polymer resins, isotropic mesophase pitch, preceramic SiC resins or a combination of these to form a multi-component matrix. Their approach would impregnate the fibrous network with liquid precursor mesophase resin in a vacuum/pressure tank and then the mesophase beginning matrix heated to solidification. Densification would occur over several cycles of preceramic polymer impregnation followed by pyrolysis creating a 'bimatrix' system. Other companies and other methods might use CVD (chemical vapor deposition) or more precisely, CVI, chemical vapor infiltration with gases such as pyrolytic carbon, SiC or other desired gases. While porosity is undoubtedly contained within the matrix, the bulk of the porosity as well as the largest pores will tend to be located at, near or associated with the intersections between multi-directional fiber bundles within the preform article since these intersections are so prominent throughout these types of configurations. Figure 4[1] highlights these areas in an *n*-D preform similar to the composites XYZ developed for evaluation in the Launch Abort Motor or System (LAS).

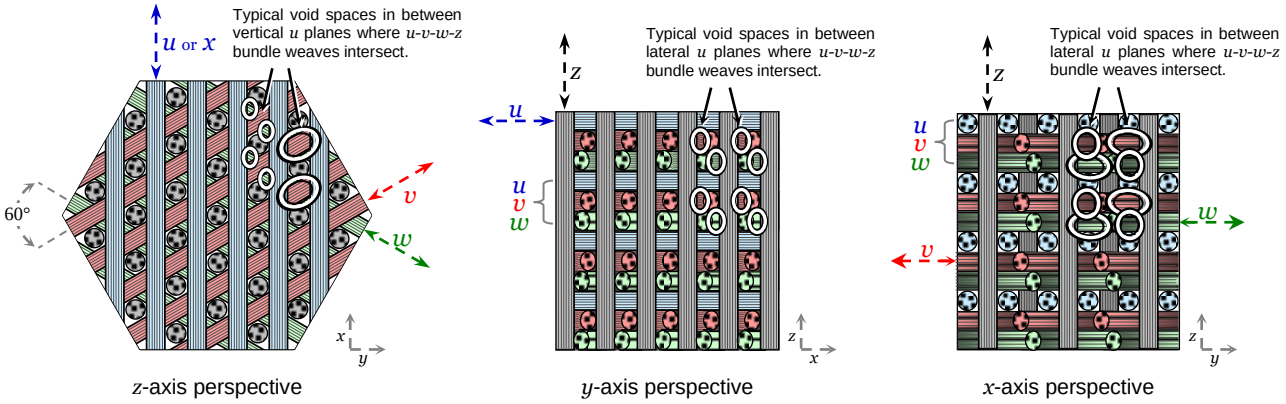

Figure 4. Cross-sectional views of the preform weave architecture similar to that used for the LAS motor looking down the *z*, *y* and *x* axis.

Figure 4 is only an illustration indicating where voids have been identified in past analyses associated with the reinforcement fiber bundle intersections. It does not take into account or reflect any pores that are present within the bimatrix phases. For these types of products, porosity can be expected to be generated in the pyrolyzed pitch phase which becomes anisotropic pitch during pyrolysis. This phase likely attains some degree of graphite-like structures within but requires 4000°F or greater to form true graphite throughout. The SiC phase converts into an amorphous SiC structure (a-SiC) around 1500°-1600°F and then to crystalline β-SiC around 3000°F. Porosity characteristics of the various phases are discussed starting with the section "Open (Liquid-Permeable) Porosity: Functional Characterization & Estimations" presented later in the report.

[1] All technical descriptions and illustrations throughout this paper are the interpretation and handiwork of the author except where noted or understood.

Relevant density ranges and values analogous to those in XYZ's C-C/SiC composite system are given in Table 2 below. Most of these have ample confirmation either from experts in the particular fields, from the literature, by independent verification and/or they were augmented using educated resources. It is important to realize the differences between the principal density classifications, in particular, what each means in terms of permeability towards the various media they encounter in the processing environments they are exposed to. That is the nature of some of the discussions that follow.

Table 2. Functional densities for primary constituents in possible C-C/SiC-based systems.

	HS40 Carbon Fiber (Mitsubushi Pyrofil 12K tow PAN)	Glassy Carbon Matrix (charred rigidization polymer)	Pitch Coke Matrix (hardened mesophase pitch carbon)	Amorphous a-SiC (SMP-10 polymer processed to < ~2200°F)	Crystalline β-SiC (SMP-10 polymer processed to > ~2200°F)
Bulk Density (liquid permeable)	~ 1.85 g/cc	1.4-1.5 g/cc	1.3-1.4 g/cc	2.4-2.5 g/cc	2.9-3.0 g/cc
Helium Density (gas permeable)	N/A	1.7-1.9 g/cc	1.96-2.07 g/cc	N/A	N/A
X-Ray Density (crystal density)	~ 2.03 g/cc	N/A	2.11-2.24 g/cc	N/A	3.21 g/cc
Absolute Density (theoretical density)	2.26 g/cc	2.26 g/cc	2.26 g/cc	3.21 g/cc	3.21 g/cc

– HS40 Carbon Fiber: This bulk density value was taken directly from the Mitsubishi product data sheet for their custom-made Pyrofil HS40 carbonized PAN fiber. In all likelihood, Mitsubishi scientists measured the apparent fiber density via ASTM D-3800 which is the industry standard Archimedes-type density test method for carbon fibers. Both PAN and rayon fibers are non-graphitizable carbon forms, and while some regions may settle into very organized 2-D graphene structures after high temperature treatments, true *d*-space indexing is nonexistent as these turbostratic configurations tend to resist 3-D graphitization, regardless of the temperature applied (graphitizable fibers include those derived from mesophase pitch precursors and pyrolytic CVD, the former undergoing graphitization after oxidative stabilization and the latter forming single crystalline graphite during the deposition process). The x-ray density given here is an average value reported by researchers at the University of Sao Paulo[1]. It is typical for this grade of PAN fiber and is reflective of some of the highly ordered and localized diffraction regions within the particular test samples examined. Most experts recognize that closed pores and micro-voids comprise a substantial quantity within the bundles and filaments of essentially all fibers, particularly carbon fibers. Intra-bundle or inter-filament pores are often tubular in shape and impervious to liquids (not to be confused with the large *inter*-bundle voids which tend to agglomerate around bundle weave intersections). The x-ray density may be closer to the density available to He atoms but the measured bulk density of 1.85 is considered to be the effective density that matrix resins encounter as they infiltrate the substrate.

[1] "Mechanical Properties and Structure of Low Density Carbon Fibers", C.J.R. González Oliver and H.A. Zolotucho, Institute of Physics - University of Sao Paulo

– Glassy Carbon Matrix: Pyrolysis of the thermoset polymer resin used to rigidize the dry preform leaves a thick deposit of glassy (vitreous) carbon throughout the open pore walls of the preform and apparently comprises part of the total carbon matrix fraction in the C-C/SiC system. All high crosslinked thermosets carbonize down to about the same char density, yielding a carbon residue that is completely non-graphitizing (glassy carbons may indeed be the least graphitizable carbon forms known; both rayon and PAN carbon fibers are made from thermoset polymers which consist mainly of glassy carbon. Crosslinked thermosets will not graphitized even when subjected to >4000°F unless high pressure or stresses are applied concurrently.

The bulk density given here has been independently determined many times (using both the ASTM C-20 water boil and impregnation techniques) and this value/range is now well substantiated within the industry [1]. Small angle x-ray scattering has confirmed a substantial fraction of hermetically sealed spherical pore volumes in glassy carbons which are impossible to breach nondestructively, even with He atoms [2] (the data also suggests that this sealed volume is equivalent to the difference/error between the measured density and the theoretical density of 2.26). Thus, it follows that little, if any, of the pore volumes in this monolith are interconnected or accessible as indicated by the He density given in Table 2, which was derived from data generated in some of Peter Harris' work [3]. The bulk density given here has been shown to represent the effective density relevant to subsequent liquid impregnations and is considered as such for the pending impregnation with pitch resin.

– Pitch Coke Matrix: Generally, both coal tar and petroleum-based pitches will undergo polymerization as they are heated and then pass into an isotropic liquid crystal mesophase state around 700°-900°F before solidifying into an inorganic, pseudo-amorphous carbon structure. It will remain in this disordered state until being subjected to > 4000°F when graphitization becomes predominant (most C-C/SiC systems never see these temperature levels during processing or their service lives, so the carbon phase never crystallizes). Mesophase pitch is preferred for forming composite binders and fibers, and since coal tar pitches are richer in aromatics, produce higher carbon yields and exhibit higher levels of solvent insolubles, their mixtures typically contain a greater fraction of mesophase precursors. In either case, the apparent (bulk) density of carbonized pitch mixtures is on the same order as that for glassy carbons as indicated in work done by researchers from Koppers Inc.[4]. Literature sources providing representative helium densities for these types of pitch-derived carbons [5] indicate substantial micro-interconnectivity throughout the pore network with very little closed porosity as indicated in x-ray densities [1] or glassy carbons. Thus, the bulk densities shown in Table 2 for both the pitch coke and glassy carbon fractions are considered to be the effective densities relevant to all subsequent impregnations with SMP-10 resin.

[1] Reference data SPI Vitreous Carbon Products and Tokai Glassy Carbon Products USA. "Small-Angle X-Ray Scattering from Glassy Carbon", W. S. Rothwell

[2] "The Effects of Particle Size on Small Angle Neutron Scattering From a Granular Phenolic Resin Char",J.M. Caloand P.J. Hall, Dept. Chem. Eng, Brown University.

[3] "New Perspectives on the Structure of Graphitic Carbons",Peter J. F. Harris, University of Reading, Whiteknights, Reading, RG6 6AF, UK.

[4] "Development of Anode Binder Pitch Laboratory Characterization Methods", E. R. Mchery, J. T. Baron and K. C. Krupinski, Koppers Industries Inc, Pittsburgh, PA

[5] "Development of Binder Pitches from Coal Tar Extract and Coal Tar Pitch Blends", Peter G. Stansberry and John W. Zondlo, West Virginia University.

Processes involved during the carbonization of pitch include the volatilization of low molecular weight constituents in the pitch and polymerization and condensation reactions of the hydrocarbons. Concurrent with dehydrogenative polymerisation, mechanisms also include hydrogenation, fragmentation and alkylation of the intermediates. Thermal cracking of the aliphatic side group at the alpha position in the aromatic molecules leads to the formation of free radicals. These aromatic free radicals react together to give aryl-aryl linkages, building up the polyaromatic molecules to form a carbonaceous liquid crystal mesophase. Higher carbon yield and lower mass loss after heat treatment is preferable. Isotropic mesophase pitches are characterized by standard procedures, which include elemental analysis, softening point and solubility tests. Since the pitch is a super cooled liquid, the transition from solid to liquid is not very distinct and the pitch does not have a true melting point but it gradually softens and becomes less viscous with increasing temperature.

– Amorphous (glassy) a-SiC is not the same as crystalline (hexagonal) α-SiC: This unusual form of SiC is uniquely derived from crosslinked pre-ceramic polymers (including the carbosilanes, silazanes and siloxanes) at lower pyrolysis temperatures and is stable up to about 2000°-2200°F when it begins to crystallize (into β-SiC). The SMP-10 pre-ceramic polymer backbone consists of an alternating carbon-silicon sequence with pendant allyl (propenyl) side groups which incorporate unsaturation into the structure permitting curing/crosslinking (via free radical addition) to harden the polymer resin prior to pyrolysis. There is evidence obtained independently and collectively indicating that less-than-optimal performance properties are achieved when this intermediate curing step is omitted. In either case, when the pyrolysis temperature is kept under about 700°- 900°F, the carbo-silane units solidify into a glassy structure, analogous to the glassy carbons derived from thermosetting organic polymers (as mentioned above). There is not much information available concerning the material science of a-SiC since it is an usual, intermediate form of SiC. The bulk (apparent) density shown in Table 1 was personally acquired from Starfire's inventor/vendor of the SMP-10 polymer and is considered to be the effective density relevant to subsequent liquid intrusions during processing.

– Crystalline (Beta) β-SiC: When a-SiC is subjected to higher firing temperatures (greater than ~3000°F, (depending on time exposure), the glassy structure rearranges and converts into its alpha form (α-SiC) followed conversion into a its face-centered cubic configuration designated as β-SiC. This process of crystallization causes volumetric shrinkage which opens up most of the previously closed voids and creates additional porosity – all open to the outside. The bulk density is reflective of the openness exhibited by the porosity. This value/range has been independently determined and also confirmed by Starfire scientists. The x-ray density has been reported as an industry standard and confirmed by numerous researchers [1].

Bulk densities for all the preceding constituents can be utilized to estimate parameters virtually impossible to acquire directly or by other means, such as the distribution of partial matrix fractions or a complex multi-component density (bimatrix, trimatrix, etc.). The other densities listed here can be used to estimate parameter values in hypothetical cases involving densification extremes and limits. Some of this will be demonstrated later.

[1] "The Strength of Moissanite", Jianzhong Zhang, Lipingwang and Donald Weider, Center for High-Pressure Research, University of New York at Stony Brook.

The physical properties of bimatrix densified C-C/SiC hybrid composites seal coated with SiC which are produced by many companies may have similarities to those from XYZ. Most of these properties have been confirmed by personal experiences. Consider a billet which undergoes 13 PIP cycles (each consist of polymer impregnation, cure and pyrolysis to about 1500°F). Finally, the substrate is 'sealed' by applying 3 or 4 PIP cycles which impregnate SiC (pre-polymer liquid form) into the remaining substrate *open* porosity. Each seal cycle consists of SiC liquid polymer impregnation, cure, pyrolysis to about 1500°F which converts the SiC structure into its glassy (amorphous) form and then fired at about 3000°F to convert the glassy SiC into it's α-SiC crystalline form. The SiC layers protect the (mainly) carbon substrate from oxidation. The average fiber volume fraction of the uncoated substrate could be represented as $f_v \sim 42.5\% - 44.7\% = 43.6\%$ (after 13 PIP cycles, prior to the first SiC seal coat). The nominal *ceramic* matrix fraction prior to coating is usually about $m_w \sim 40\%$ (this does not include the C/C fraction deposited early in the process). The nominal bulk substrate density after the C/C densification stage could be $\rho_{b,0} \sim 1.02 - 1.28 = 1.15$ g/cc (clarification of subscript designations utilized in this study are articulated in Appendix A). The average (multi-component) bulk density of the substrate at the end of the formal densification stage (after PIP cycle #13, prior to Seal Coating) can be represented as about $\rho_{b,13} \sim 1.70 - 1.78 = 1.74$ g/cc. The average open porosity of the densified substrate (after PIP cycle #13, prior to Seal Coating) can be estimated to be about $p_{o,13}$ 11.0% – 15.0 = 13%. Finally, the nominal thickness of SiC coating applied by hand-brushing (assuming 4 SiC PIP seal coats) could be represented as $t \sim 0.003 - 0.007 = 0.005$" thickness. Table 3 below summarizes these averages for reference . . .

Table 3. Nominal and average property values for common C-C/SiC material systems.

Average Pre-Coat Fiber Volume Fraction	Nominal Pre-Coat SiC Matrix Weight Fraction	Nominal Bulk Density after C/C Densification	Average Pre-Coat Bulk Density	Average Pre-Coat Open Porosity	Nominal Thickness of Seal Coat Layers 1-4
43.6%	~ 40%	1.15 g/cc	1.74 g/cc	~ 13%	0.005"

It was not possible to conduct or oversee any independent testing of XYZ's process which may have helped to confirm, refine or refute these data, however, the stated fiber volume fraction, bulk densities and porosity data are reinforced from other information made available or by direct correlations with related data. Some of these corroborations will be explored shortly. Total and partial matrix contents in these types of composites are next to impossible to measure physically. Since this system is not susceptible to more accepted quantification methods such as resin content analysis via acid digestion, special estimation techniques must be pursued. Now, to be consistent with XYZ's designations, the pre-coated state is considered to refer to the substrate which has formally been processed through several PIP densification cycles (likely 12 or 13), while the coating phase consists of all the embedded and deposited material beyond PIP #13, namely, seal coats 1 through 4.

Company XYZ indicated that a graphical data plot of the substrate bulk density was physically measured by XYZ technicians/engineers at each of the pyrolyzed states throughout the densification process. This is typically performed during these types of operations. The author has conducted

numerous such work and analysis of similar C-C/Si hybrid test articles in previous studies generating bulk density, impervious density, matrix content and fiber volumes among other relevant properties. Such experience has been adapted to generate representative plots from other companies, including XYZ to some extent. This approach intends to reflect the incremental and cumulative behavior of the substrate bulk density and other critical properties as they gradually increase after each substrate PIP densification cycle. Since the data likely parallels that generated by XYZ and other companies containing side-by-side density and open porosity values, it is likely that XYZ employed techniques used by the author and other companies to obtain rough estimates reflecting state-by-state density/porosity estimates such as one of the Archimedes/buoyancy technique for instance. Figure 5 in the next section provides a representative pattern indicate how the bulk density varies throughout the process.

Bulk Density: Functional Characterization & Estimations

It is obvious from Figure 5 that the greatest weight gains occur in the first few cycles which gradually taper off after many cycles have been completed. Independent studies have meticulously demonstrated and established[1] that this behavior can be tracked precisely and repeatedly along a generalized response function of the type . . .

$$P = A\left(1 - e^{-ki}\right) + C$$

or specifically for the C-C/SiC bulk density . . .

$$\rho_{b,i} = \left(\rho_{b,\infty} - \rho_{b,0}\right)\left(1 - e^{-ki}\right) + \rho_{b,0}$$

where $\rho_{b,i}$ is the composite bulk density at any given pyrolyzed state *i* along the densification path; $\rho_{b,\infty}$ is the bulk density after an infinite number of densification cycles (if that were possible); and $\rho_{b,0}$ is the bulk density at the beginning of the ceramic densification process, after the C-C matrix phase has been incorporated into the substrate. Thus, while the weight gains become smaller and smaller, the incremental (step-by-step) increases in bulk density also become smaller . . . as the bulk density asymptotically approaches a hypothetical maximum or threshold density at $\rho_{b,\infty}$.

The that the density tracking data given in Figure 5 has been substantiated numerous times over the years by the author to closely reflect the actual values obtained by individual testing of most of the properties using physical testing with formal and modified ASTM practices, It is believed the estimated mated and above is a experimental plot depicting multiple densification runs performed by XYZ on various billets, slabs and test articles during their development work for the C-C-SiC product concept. This data is re-plotted in Figure 5 below, less the two 3000°F HT states, but including the two additional density states ($\rho_{b,-2}$ and $\rho_{b,-1}$) and a precisely modeled curve fit. The resulting model functional expression also follows . . .

[1] Derivation and proofs for such concepts have already been developed, substantiated and long established – Please consult Appendix A for further clarification.

Figure 5. Re-plot of the data in Figure 1 along with a precise model fit and two new points of interest.

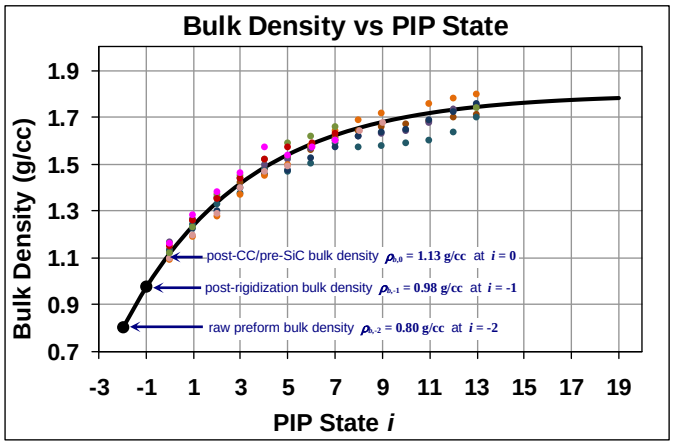

$$\rho_{b,i} = 0.68\left(1 - e^{-0.2i}\right) + 1.13$$

Figure 5 applies a general characterization approach for PIP processes independently developed and validated in previous R&D studies conducted hundreds of times for density, matric content and porosity as will cover later. It was eventually shown that reverse exponentials or Weibull exponentials were best for indicating and the theoretical upper limit to the number of PIP cycles which would be needed to be needed reach zero porosity which can never be attained since even the very last cycle would leave some porosity in to component for these types of materials (see the Appendices). Here, the bulk density at the C/C state (i = 0) is given as $\rho_{b,0}$ = 1.13 g/cc (in good agreement with the value in Table 4 below). The bulk density at infinite densification (if that were possible) would become $\rho_{b,\infty}$ = 0.68 + 1.13 = 1.81 g/cc. Values are tabulated for selected model states in Table 4 below. The model predictions in Table 4 appear to be in good agreement the estimated values provided in the following sections.

Table 4. Selected points of interest along the C-C/SiC bulk density model curve.

Dry Preform State i = -2	Rigidization State i = -1	Carbon Pitch State i = 0	1st Ceramic State i = 1	5th Ceramic State i = 5	10th Ceramic State i = 10	13th Ceramic State i = 13	∞th Ceramic State i = ∞
0.80 g/cc	0.98 g/cc	1.13 g/cc	1.25 g/cc	1.56 g/cc	1.72 g/cc	1.76 g/cc	1.81 g/cc

Note that $\rho_{b,\infty}$ = 1.81 g/cc at $i = \infty$ is projected to be the average maximum bulk density achievable for this material system under the particular fabrication conditions applied and raw materials incorporated (relative to the *open* porosity, of course). This bulk density upper limit is accompanied by a corresponding average minimum limit for the open porosity and an average maximum limit for the true density. Both of these parameters will also be developed shortly. It should be emphasized here that this is the *average* maximum bulk density with respect to the collective series of data curves the analysis given in sections that follow. Individual slabs and articles can exhibit higher or lower curves giving threshold bulk densities that can range anywhere from about 1.70 to 1.85 g/cc.

It should be realized that each densification cycle associated with essentially all PIP-type process approaches accomplishes two effects . . . (1) Permeation and densification of open, accessible pores and cavities, and (2) Closing and sealing of pore tunnels and narrow interconnects leading to larger cavities which were formerly accessible. Unfortunately, a certain level of pores are closed off during each densification cycle. The partial fractions of open and closed porosity vary from cycle to cycle and there are indications that the fraction of trapped pores increases with each cycle. Thus, the surmised true density at any given state must contain this 'error', and as long as closed pores and voids are created with each cycle, the bulk density will never come close to the true density.

Immediately after dry weaving, the preform must be rigidized in order to prevent deformation or damage to the fibers which can be imparted during handling and subsequent processing. There is not enough information available to fully substantiate the exact rigidization process XYZ utilized on the freshly woven preform structure. However, examination of some of the photos provided strongly suggests that rigidization was accomplished by restraining the billet preform in a specially fabricated cage assembly using a low viscosity liquid thermoset polymer which was allowed to passively soak into the preform structure and harden (crosslink) at room temperature. A number of polymer types could be used for this purpose where the preform structure is essentially casted in an opaque plastic and then carbonized to yield a thick glassy carbon fiber coating which appears to constitute a significant portion of the total carbon matrix fraction. Pyrolysis of the casted preform containing these types of thermoset polymers would only yield a small char residue but would leave a very open (and rigidized) porous structure for safe pitch resin impregnation. This initial carbon deposit will permanently remain in the glassy state since glassy carbon forms are non-graphitizing structures.

After rigidization of the preform, pitch densification can then be carried out using more aggressive processing/handling techniques including high temperature, vacuum and pressure and physical manipulation with heavy duty cranes and fixturing hardware. For the processing scenario under consideration, following rigidization and pyrolysis of the as-fabricated pre-form billet, a single pitch impregnation/ followed by a ~3000°F firing cycle is applied which converts the liquid pitch mesophase into a semi-hardened isotropic mesophase carbon structure. This insures that the carbonized pitch fraction is left in an amorphous hardened mesophase state. If applied, a 4000°F heat cycle would essentially graphitize this carbon fraction into solid hexagonal graphite. However, many C-C/SiC substrates never see this level of temperature. Thus, the carbonaceous phase may be comprised of a mixture of two sub phases (or partial fractions) . . . glassy carbonized rigidized polymer plus a carbonized isotropic mesophase pitch phase. Other than the 2-D graphene layers which may be present to some degree, the carbonaceous multi-phase would contain no 3-D crystallites and is pseudo-amorphous throughout.

For both 2-D and 3-D type composite structures, geometrical volume changes after the rigidization or laminate molding process have been documented to be infinitesimal or immeasurable throughout the densification process. For 2-D laminated systems, volume shrinkages on the order of 2% in the thickness direction may occur during the first pyrolysis cycle going from the molded state to the first C/C state. Beyond this cycle however, volume changes are immeasurable, infinitesimal or nonexistent. For 3-D composite systems, in particular the C-C/SiC system, the weaving process establishes all three dimensional boundaries and unit cell parameters of the preform structure at the onset and then the rigidization process permanently fixes these attributes in space.

Thus, it should be recognized that the fiber volume fraction (or 'fiber volume') of all C-C/SiC articles is permanently established in the billet state before any densification cycles are ever applied and it remains invariant from that point on (only changing slightly after the coating phase is applied). As such, the Table 3 value of $f_v = 43.6\%$ is considered to be the constant average fiber volume fraction of C-C/SiC articles . . . since *the substrate volume remains constant throughout the entire process*, so does the fiber volume. However, the fiber *weight* fraction f_w is not constant because it gradually increases over the process in accordance with the decreasing matrix weight fraction m_w, a fact that is exemplified by the rule [1] . . . $f_w + m_w = 1$. This helps to facilitate the understanding that substrate densification is most appropriately defined as *matrix densification.*

For the C-C/SiC system, the fiber volume can be directly estimated before any processing begins by obtaining accurate measurements for the dry billet (preform) weight W_{-2} and corresponding geometrical volume V (the constant substrate volume $V = V_{-2} = V_{-1} = V_0 = V_1 = V_2 = etc...$). If measurements are carefully taken, the bulk density in the dry preform state $i = -2$ can be determined. On the average, this turns out to be $\rho_{b,-2} \simeq 1.81$ g/cc (from Table 4). In this process state, the HS40 fibrous preform is the only reinforcement weight constituent present, that is, $f_{w,-2} = 1$, and so the fiber volume is estimated simply by using Mitsubishi's measured (average) fiber density $\rho_f = 1.85$ g/cc, from Table 2 and the bulk density of the dry preform structure, that is . . .

$$f_v = f_{w,-2}\,\frac{\rho_{b,-2}}{\rho_f} = 1 \times \frac{0.81\ \text{g/cc}}{1.85\ \text{g/cc}} \simeq 43.6\%$$

For organic-based PMC systems, the resin content (matrix weight fraction) at the molded (post-autoclave) state can be directly measured using such robust tests as ASTM nitric acid digestion, but this technique is ineffective for pre-ceramic (semi-organic) polymers. Thus, from this point on, quantities such as matrix content, matrix volume and matrix density must be obtained indirectly by estimations based on weights and geometrical dimensions (for the current study at hand, the bulk density values given in Figure 6 below are the only data available for this purpose). Partial matrix fractions and the composite matrix density are complex, requiring even more intricate estimation techniques to yield useful and productive values (as covered in Appendix B and C). It goes without saying, any meaningful analysis in this regard is entirely at the mercy of the good techniques practiced by the floor engineers and technicians responsible for precisely measuring these raw parameters.

[1] See Appendix A to better understand the discussions in these sections and the subscript nomenclature used.

A more robust approach would include both of the 3000° heat treat steps after PIP cycles 5 and 10. This would call for a more complex characterization of the data in multiple segments rather than a single function, but it would improve tracking accuracy along with more precise projections near the extremes. For demonstration purposes, omitting these two HT states does not introduce enough error to substantially affect the results. However, as will be seen shortly, effective characterization of the porosity here will require at least an elementary estimation of the partial matrix fractions and the complex matrix density from which the 3000° HT points will be taken into account.

Matrix Content: Functional Characterization & Estimations

The raw bulk density values provided in Figure 5 can be used for estimation of other constituent quantities relevant to the C-C/SiC system as it undergoes densification processing. For instance, using Eq(3A) given in Appendix A or Eq(5B) in Appendix B, the total matrix content m_w at any densification state i can be estimated directly from the corresponding bulk density value at the same state $\rho_{b,i}$, that is as shown in Figure 7 and Table 5 . . .

$$m_{w,i} = 1 - f_v \rho_f \rho_{b,i}^{-1} \qquad \text{or} \qquad m_{w,i} = \left[1 + \rho_{b,-2}\left(\rho_{b,i} - \rho_{b,-2}\right)^{-1}\right]^{-1}$$

Figure 7 gives a plot of data generated from either of these formulas directly from the measured bulk densities along with a precise model fit best describing its behavior.

Figure 7. Total matrix content and model fit across the process estimated directly from the bulk density data in Figure 2.

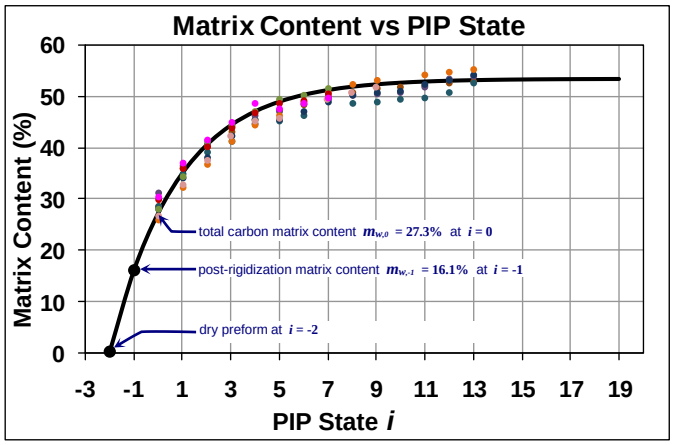

$$m_{w,i} = 26.2\left(1 - e^{-0.354i}\right) + 27.3$$

At the state $i = 0$, the matrix contains only inorganic carbon and its content is estimated to be $m_{w,0} = 27.3\%$. As with the bulk density model, the total matrix content after an infinite number of densification cycles (the threshold matrix content) is given simply as $m_{w,\infty} = 26.2 + 27.3 = 53.5\%$. Model values are tabulated for selected states in Table 5 below . . .

All technical descriptions from previous work and analytical approaches throughout this paper are the experience and handiwork of the author except where noted.

Table 5. Selected points of interest along the C-C/SiC total matrix content model curve.

Total Matrix Content

Rigidization State i = -1	Carbon Pitch State i = 0	1st Ceramic State i = 1	5th Ceramic State i = 5	10th Ceramic State i = 10	13th Ceramic State i = 13	∞th Ceramic State i = ∞
16.1 %	27.3 %	35.1 %	49.0 %	52.7 %	53.2 %	53.5 %

Here, $m_{w,\infty}$ = 53.5% is projected to be the average maximum total matrix content achievable for this material system under the particular fabrication conditions and raw materials incorporated. Again, this is the *average* maximum matrix content with respect to the collective series of data curves given in Figure 7 – individual slabs and articles will exhibit higher or lower curves giving maximum total matrix contents that can range anywhere from about 50 to 57%.

At any state during the densification process, the total matrix content is the sum of partial fractions comprising a 'quadmatrix' consisting of varying amounts of: (1) carbonized rigidization polymer (glassy carbon), (2) carbonized mesophase resin (amorphous carbon), (3) amorphous/glassy silicon carbide (a-SiC), and (4) crystallized cubic silicon carbide (β-SiC). The combination of fractions (1) and (2) make up the total carbon content while the combination of (3) and (4) comprise the total SiC portion of the total 'bimatrix'. Comprehensive estimations for the partial matrix fractions in the C-C/SiC system and the technique used are given in Appendix B. The graphical and tabulated results provided in Appendix B reveal an interesting distribution for each of the four co-constituents comprising the total matrix phase within the C-C/SiC system. Results for selected states calculated from the bimatrix model in Appendix B are given in Table 6 below . . .

Table 6. Selected points of interest along the C-C/SiC bimatrix content model curve given in Appendix B.

Bimatrix Content

	Carbon Pitch State i = 0	1st Ceramic State i = 1	5th Ceramic State i = 5	10th Ceramic State i = 10	13th Ceramic State i = 13	∞th Ceramic State i = ∞
Total C	28.3 %	25.3 %	18.8 %	16.3 %	15.8 %	15.4 %
Total SiC	0.0 %	9.3 %	28.7 %	36.0 %	37.3 %	38.4 %

Values determined from this approach (Appendix B) are in fair agreement with those provided by the total matrix content model developed above in Table 5 (recall the total matrix content at any state is simply the sum of the carbon and SiC fractions at that state; the C fractional content gradually decreases as the SiC content increases across the process). Incidentally, the bimatrix model projection implies that the total carbon content at the end of the process and beyond is about 15-16% while the total SiC content never completely reaches the 40% level.

The corresponding open porosity fraction $p_{o,i}$ at any state i can also be estimated directly from the raw density values given in Figure 1 by using Eq(7A) or (8A) developed in Appendix A . . .

(8A) $$p_{o,i} = 1-\rho_{b,i}\rho_{m,i}^{-1} - f_v\left(1-\rho_f\rho_{m,i}^{-1}\right)$$

However, before these estimations can be carried out, corresponding values for the *matrix density* must be determined. For the C-C/SiC system, the matrix density is physically complex since it consists of four co-constituents each of which vary from state to state. It is a composite density in which a functional bulk density for each matrix co-constituent must be ascertained. This is difficult because 'bulk' densities are automatically dependent on the particular materials, processes and conditions to which the parameter is associated or measured. The bulk constituent densities given earlier in Table 2, page 8 were presented with emphasis to the C-C/SiC and like systems. Generalized bulk density can be ambiguous since its volume boundaries are often specified by the test methods used to define a given system (i.e... pour density, tap density, foam density, apparent density, etc . . .).

Before the incremental composite matrix densities can be determined however, the distribution of partial matrix fractions for each of the co-constituents must be developed. The techniques used to estimate partial matrix weight fractions and the composite matrix densities are given in Appendices B and C respectively, along with their results. Table 6 above presented a small portion of this analysis. All that will not be rehashed here. Rather, with representative estimates for the matrix density at hand, the open porosity fraction for the C-C/SiC system can be evaluated similarly to the functional descriptions for substrate bulk density and the total matrix content developed above. Using the raw density values given in Figure 5, and the formula above, a corresponding plot and model curve for the open substrate porosity fraction are given in Figure 8 below followed by the representative response function which best describes its behavior . . .

Figure 8. Open porosity fraction and model fit across the process estimated directly from the bulk density data in Figure 2.

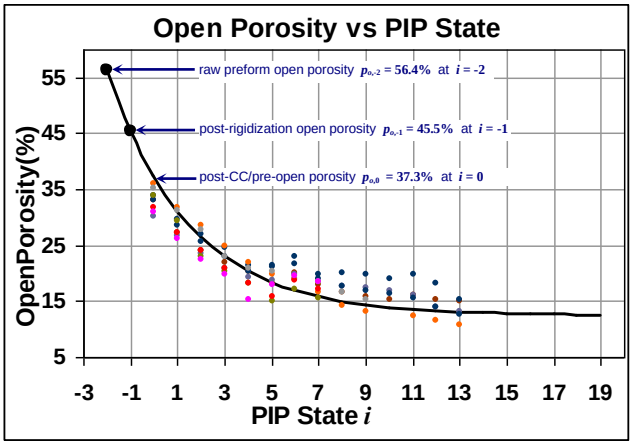

$$p_{o,i} = 24.9\, e^{-0.285i} + 12.4$$

At the state $i = 0$, the open porosity fraction is indicated to be $p_{o,0} = 21.8 + 13.1 = 37.3\%$, while its value after infinite densification (if that were possible) is simply $p_{o,\infty} = 12.4\%$. Model estimates for selected states are tabulated below in Table 7. Results for the states $i = -2$ and $i = 13$ are in excellent agreement with measured values.

Table 7. Selected points of interest along the C-C/SiC open porosity model curve.

Open Porosity

Dry Preform State i = -2	Rigidization State i = -1	Carbon Pitch State i = 0	1st Ceramic State i = 1	5th Ceramic State i = 5	10th Ceramic State i = 10	13th Ceramic State i = 13	∞th Ceramic State i = ∞
56.4 %	45.5 %	37.3 %	31.1 %	18.4 %	13.8 %	13.0 %	12.4 %

Here, $p_{o,\infty} = 12.4\%$ is projected as the average minimum open porosity achievable for this material system under the particular fabrication conditions and raw materials incorporated. Note that in the dry preform state (at $i = -2$), before densification processing begins, the pre-determined fiber volume fraction $f_v = 43.6\%$ implies an initial open substrate porosity of $p_{o,-2} = 56.4\%$. Also note that at the end of densification (at $i = 13$), approximate open porosity values for the C-C/SiC material were previously documented by XYZ/ATK engineers to be around ~13%. Both of these correlations serve to strengthen the validity of these models. Again, bear in mind that $p_{o,\infty}$ is the *average* minimum open porosity with respect to the collective series of data curves given in Figure 5, page 12 – individual slabs and articles will exhibit higher or lower curves resulting in minimum (threshold) open porosity fractions that can range anywhere from about 9 to 17%.

For liquid-densified (PIP-densified) C/C and CMC systems, the threshold porosity can never actually be taken to zero . . . there will always be some residual open porosity in the substrate after each densification cycle. This is because each cycle ends with a pyrolysis step which creates new pores, voids and cavities due to the expulsion of pyrolysis volatiles in combination with substantial volumetric shrinkage of the matrix material as it undergoes thermal conversion. For SMP-densified systems, this corresponds roughly to about 20% loss in polymer during pyrolysis and a 50% shrinkage of the remaining matrix during conversion into ceramic. For the current C-C/SiC system under study, this leads to a threshold porosity that approaches the ~12% level. In addition to the open (liquid-permeable) porosity, the density-porosity relationship includes a distinctive bulk (liquid-permeable) density and an associated 'true' density which pertains to the liquid-impermeable or impervious portion of the material as simply defined by . . . $\rho_b = (1 - p_o)\rho_t$.

In all systems of this type, the total porosity gradually decreases with each densification cycle but changes in the open and closed porosity fractions are not necessarily equivalent. There are some indications that the partial fraction of closed pores actually increases from state-to-state at the expense of the open porosity. This 'error' is inevitably built into the actual values obtained during physical measurements of bulk density and open porosity. Additionally, it is all but certain that reported XYZ density/porosity values for their 3-D C-C/SiC material were determined using one of the Archimedes techniques on cubic-shaped test samples in which all six sides were machined to form the sample. This permits all six faces to reflect approximately the same inner pore structure which, because of the machining effects, exposes a mixture of both open and closed pores. In contrast, test samples

extracted from 2-D composite laminates or panels usually consist of four exposed cross-sectional edges representative of the panel thickness (in-plane), and two larger faces (the processed mold side and bag side surfaces), which are partially sealed and less pervious than the cross-sections. The errors reflected in these two sample configurations should not be overlooked.

In any case, the continuation of additional densification cycles at the high end of the curve in efforts to try and fill up the last few percentages of open porosity is not cost-effective because a point of diminishing returns is reached far below the theoretical threshold porosity. However, it might be interesting to consider some of the benefits or effects that a 14th cycle might have using alternative densification techniques or matrix materials. For instance, chemical vapor deposition/infiltration (CVD/CVI) is carried out by 'cracking' gaseous reactants in a hot, evacuated chamber containing the porous article, but its ability to penetrate the deepest pores is highly sensitive to the process conditions utilized (pressure, reactant composition, temperature, residence time). CVD/CVI is commonly used to deposit polycrystalline β-SiC and quasi-amorphous pyrolytic carbon during densification and coating operations. While this method is effective at densifying the outer most micro- and meso-pores, many of the large pores and voids, such as those at the fiber bundle intersections are difficult to fill up. Additionally, CVD/CVI deposits have a tendency to accumulate faster around the pore openings and edges, often completely closing off pore tunnels leading to the interior. Both of these effects result in higher (and undesirable) levels of closed porosity. While CVD techniques have a long history throughout the C-C/CMC industry, densification of fibrous composites via forced-flow isothermal CVD/CVI has been utilized extensively in recent years, offering slightly improved deposition/infiltration effects which typically reach threshold porosities that can range anywhere from about 8% to 15% (not all too different than the current C-C/SiC system under study).

Techniques for deposition of glassy carbons via liquid (polymer) impregnation, thermoset crosslinking and pyrolysis (PIP) (similar to the rigidization process discussed earlier) also have a long history, including the archaic but highly successful RCC/ACC systems. This practice uses the same approach as XYZ's PIP process for their C-C/SiC material except pyrolytic volume losses for cured phenolic polymer are not nearly as high as that for SMP-10. That is, fewer densification cycles are required to reach the appropriate density level (and corresponding mechanical strengths), and the threshold porosity is lower . . . threshold porosities for phenolic-densified 3-D PAN-based C/C systems have been independently determined to be in the 7-9% range and are primarily due to large voids at the fiber bundle intersections. Unfortunately, PIP-type densification methods also have a tendency to block off pores – but to a lesser degree than most CVI/CVD approaches.

It is a matter of curiosity to wonder what the bulk density of the substrate might be if the remaining ~13% porosity in the C-C/SiC material at i = 13 was occupied with material deposited by alternative densification techniques. Of course, this would carry the substrate to the state i = 14. Appendix D includes the method for developing a simplified formula, Eq(2D), which can provide estimates of this type, namely . . .

(2D) $$\rho_{b,i} = \rho_{b,o} + \left(x_v - p_t\right)\rho_x$$

Here, $\rho_{b,i}$ is equivalent to the new or final composite bulk density $\rho_{b,14}$; $\rho_{b,o}$ represents the former density $\rho_{b,13}$ whose value can be taken as about 1.74 g/cc from Figure Table 2 (page8); x_v is the volume fraction of the newly added matrix material while ρ_x is its bulk density; and p_t is the threshold porosity indigenous to a hypothetical composite densified with the new material under consideration. Using Eq(2D), Table 8 below contains several scenarios of interest for matrix media and densification (application) methods which might be utilized to carry the porous C-C/SiC substrate from the i = 13 state to i = 14. Estimates for an organic solvent, ordinary water and a cured polymer resin (analogous to a Polymer Matrix Composite) are also given and provide an interesting comparisons for reference. As inferred by the results, the threshold porosity p_t has a very significant effect on the final composite bulk density $\rho_{b,i}$ in spite of the density exhibited by the new matrix material ρ_x. Justifications immediately follow Table 8 supporting the various ρ_x and p_t values utilized in these simulations . . .

Table 8. Final bulk composite densities expected for various scenarios with an added densification step from i = 13 to i = 14.

Densification from the state i = 13 to the state i = 14

New Material	**Glassy Carbon**	**Pitch Carbon**	**Pyro Carbon**	**β-SiC**	**Kerosene**	**Water**	**Cured Phenolic**
$\rho_{b,x}$ of Material	1.45 g/cc [1,5]	1.35 g/cc [2]	2.05 g/cc [3]	3.2 g/cc [4]	0.817 g/cc [77°F]	0.998 g/cc [77°F]	1.24 g/cc [5]
App Method	PIP	PIP	CVI	CVI	wet impreg	wet impreg	impreg/cured
Threshold p_t	p_t ~ 8% [6]	p_t ~ 10% [7]	p_t ~ 12% [8]	p_t ~ 12% [8]	p_t ~ 0%	p_t ~ 0%	p_t ~ 4% [9]
Final Composite ρ_b	1.82 g/cc	1.79 g/cc	1.77 g/cc	1.78 g/cc	1.85 g/cc	1.87 g/cc	1.86 g/cc

Table Notes:

1 - As provided in Table 2 (page 8), the liquid-permeable density of glassy carbon is about the same for all polymer thermoset precursors, including rigidization polymer, cured phenolic resin, epoxies, etc . . .

2 - As provided in Table 2, the liquid-permeable density of amorphous pitch carbon which has not been graphitized is reflective of analogous bulk densities for green coke and hardened mesophase.

3 - The gas-permeable density of CVD-deposited carbon has been determined independently and by other industry sources [1]; its deposits may consist of mono/polycrystalline mixtures.

4 - The gas-permeable density of CVD-deposited SiC has been determined independently and by other industry sources[2]; on carbon substrates, its deposits are polycrystalline.

5 - Liquid-permeable densities for cured and charred phenolic resins have been extensively characterized independently (principally Borden brand resoles and novolacs, including SC-1008HS and associated and family types).

Other Notes:

a - The sectioned porosity threshold for phenolic-densified 3-D PAN-based C/C systems has been independently determined to be in the 7-9% range and is primarily due to large voids at the fiber bundle intersections.

b - It has inferred from industry workers and researchers that the sectioned porosity threshold for pitch densified 3-D PAN-based C/C articles runs in the 10-12% range [3].

c - It has been inferred from industry workers and researchers that sectioned threshold porosity values for pyrolytic and CVI-densified materials runs in the range 8 to 18%; much of the porosity consists of closed pores and larger voids at the fiber bundle intersections which are difficult to fill using CVD/CVI approaches.

d - When impregnated effectively, liquids will occupy 100% of the open porosity in a system (this includes liquid polymer resins prior to cure). Unlike many other resins, phenolics crosslink via condensation which expels water molecules and curing volatiles. When cured properly, this leads to a unique, interconnected micro-porosity network within the phenolic phase which is almost undetectable. In a composite system however, resin/matrix shrinkage during the curing process will create larger voids and pore channels along and parallel to the fiber bundles. The threshold porosity for loosely compacted composite structures (such as those derived from 3-D preforms) has been determined independently to be around 3-5% (open threshold porosities for well compacted 2-D laminates can be as low as ~1.5%).

[1] As taken from the product data sheet for Carbograf 400 pyrolytic CVD graphite and supplemented by independent testing at Poco Graphite Inc.
[2] As taken from the product data sheet for Carbosil 100 CVD SiC coating and supplemented by independent testing at Poco Graphite Inc.
[3] "Mesophase Pitch for Low Pressure Carbon/Carbon Composite Processing", Mickael Dumont and René Pailler, University Bordeaux, 33600 Pessac, France

Hypothetically, if it were somehow possible to fully saturate the residual porosity ~13% with β-SiC (disregarding threshold porosities for the moment), the densified composite would contain zero open porosity, the bulk density and true density would coincide and the final composite bulk density would become . . . $\rho_{b,14}$ = 2.17 g/cc. But this is not possible because threshold porosities limit complete densification. At any rate, since the tool is out and being used, consider some scenarios in which the HS40 preform (substrate) is densified exclusively with a single matrix material throughout, that is, from the preform state i = –2 to the final i = 13 state. Ignoring rigidization requirements for the moment, recall that the bulk density and open porosity for the undensified, freshly woven preform are $\rho_{b,-2}$ = 0.81 g/cc and $p_{o,-2} = 1 - f_v$ = 56.4% as provided earlier. These parameters become the starting point for generating the estimates or scenarios given in Table 9 below . . .

Table 9. Final bulk composite densities expected for HS40 substrates densified with a single matrix material.

Densification from the state i = -2 to the state i = 13

Matrix	**Cured Phenolic**	**Glassy Carbon**	**Pitch Carbon**	**Pitch Carbon**	**Pyro Carbon**	**β-SiC**
Method	molded	PIP	PIP	PIP/graph	CVI	CVI
Threshold p_t	p_t ~ 4%	p_t ~ 8%	p_t ~ 10%	p_t ~ 12%	p_t ~ 12%	p_t ~ 12%
Final ρ_b	1.46 g/cc	1.51 g/cc	1.43 g/cc	1.72 g/cc	1.72 g/cc	2.23 g/cc

A couple of additional scenarios have been improvised for Table 9 to represent possible cases in which the preform was simply molded in phenolic resin and another where the carbonized pitch composite was subjected to full graphitization temperatures (4000°- 4500°F) in multiple steps across the process. All in all, these estimates are quite reflective of composite bulk densities reported throughout the literature and are supported by independent studies and resources for similar composite platforms (i.e. . . 3-D carbonized PAN reinforcements embedded in organic/inorganic carbon and SiC matrix systems). The results depicted in Table 9 could provide some interesting insights into the nature of the material if the original HS40 3-D preform was processed along entirely different routes from scratch. This approach could also be expanded to include a mixture of bi-, tri- and quadmatrix scenarios. For instance, using the premise suggested by Eq(2D) above (as taken from Appendix D), a formula for estimating the bulk composite density of the current quadmatrix C-C/SiC system under study might take the form . . .

$$\rho_b = \rho_{b,-2} + (p_{-2} - p_{-1})\rho_{cp} + (p_{-1} - p_0)\rho_{cm} + (p_0 - p_{10})\rho_{s,a} + (p_{10} - p_{13})\rho_{s,\beta}$$

where ρ_{cp} is the density of the carbonized rigidization polymer, ρ_{cm} is that of the carbonized mesophase pitch, $\rho_{s,a}$ the density of a-SiC and $\rho_{s,\beta}$ the density of β-SiC. This approach may provide a quick means for roughly estimating certain properties in composites comprised of multi-constituent matrices, but does not appear to be as precise as the method of partial fractions outlined in Appendix B.

The open (liquid-permeable) porosity can be physically measured . . . and so can the gas-permeable porosity (or helium porosity). However, it is next-to-impossible to ascertain the total fraction of *closed* porosity and hence the net or overall porosity in a given material system. As with the open porosity fraction, the partial fraction of porosity that is closed off, sealed up, plugged, blocked, occluded, covered over, impervious or otherwise impermeable to Darcy flow can consist of macro-, meso- and micro-pores, spherical voids, tubular voids, bubbles, inclusions, tunnels, dendrites, cavities, separations, delaminations and microcracks as indicated in Figure 1 earlier. Glass-like materials including glassy carbons and glassy ceramics (such as charred phenolic and SMP-10 resins) are known to contain spheroid-shaped bubble-type voids which are completely hermetic to Darcy flow. These types of closed micro-volumes have been confirmed and dimensionally measured using small angle x-ray and neutron diffraction techniques on monolithic samples of these materials.[1]

For certain multi-constituent composite systems, much of the porosity is interconnected, at least through the smallest of micro-channels. Undoubtedly, if all the porosity volume available to infiltrating He atoms was physically quantified, a substantial portion of the total porosity would be captured. Recall Table 2, page 8 which outlines various definitions or levels of density for each primary constituent in FMI's C-C/SiC system. The first row in Table 2 contains bulk density values most relevant to flowing liquids (liquid permeable densities) while the second, third and fourth rows show densities susceptible to permeating gases gas as based on helium volume measurements, x-ray (crystal) density and theoretical (estimated) crystal densities are more appropriate to electron flow and lattice-scale interactions. Note however, that test results acquired using helium pycnometry techniques provide density and porosity values which include all the liquid-permeable macro and meso-pores *in addition to* all the gas-permeable micro-pores. From a practical perspective, porosity values derived via He pycnometry could be envisioned as the *absolute open porosity*. In some situations, these results can be effectively treated as total porosities, or very near it . . . but this excludes most composite materials, particularly those containing matrices which undergo out-gassing and volumetric changes during curing or conversion processes.

Now consider a scenario in which the porosity volume of interest pertains to that fraction of the total porosity that is permeable to He atoms. This approach can follow the same analysis that was developed previously for the open porosity but using the helium densities instead. From Table 2, the following He densities for the each of the C-C/SiC constituents can be utilized: (1) ρ_f ~ 1.95 g/cc, (2) ρ_{cp} ~ 1.8 g/cc, (3) ρ_{cm} ~ 2.0 g/cc, (4) ρ_a ~ 2.8 g/cc, and (5) ρ_β ~ 3.1 g/cc respectively for the HS40 carbon fiber, carbonized rigidization polymer, carbonized mesophase resin, amorphous a-SiC and crystallized β-SiC. Justifications for these assignments are as follows . . .

(1) Many of the bundle intersections, inter- and intra-bundle voids, cavities and interstitials which eventually become impermeable to intruding liquids are actually accessible through micro-channels, allowing passage of He atoms. As a consequence, this is expected to raise the effective fiber (bundle) density substantially. (2) When fully cured/crosslinked thermoset polymers are fired, the

[1] "Small-Angle X-Ray Scattering from Glassy Carbon", W. S. Rothwell, J. Appl. Phys. 39, 1840 (1968)
[1] "The Effects of Particle Size on Small Angle Neutron Scattering From a Granular Phenolic Resin Char", J.M. Calo & P.J. Hall, Strathclyde University, Scotland, UK

ejected pyrolysis gases (primarily hydrogen along with H_2O, CO_2, CO, a number of small aliphatics and aromatics) augment the interconnecting network of micro-pores and passages throughout the glassy body but a substantial fraction of closed voids are also created during conversion from organic to inorganic carbon. As referenced earlier, the evidence clearly shows that many of these enclosed volumes are hermetic to gases and liquids. Thus, the He density is not expected to be much different than its liquid-permeable density. (3) As with glassy carbons, when pitch mesophase resin carbonizes, the interconnecting porosity network is broadened. Unlike glassy carbons however, this conversion process is *not* accompanied by the formation of hermetically sealed bubbles. In combination with volumetric shrinkage due to microstructural condensation and compaction, these two effects cause the apparent density to approach theoretical. (4) Amorphous (glassy) a-SiC formed via low-temperature pyrolysis is expected to exhibit an appreciable degree of gas hermeticity analogous to the glassy carbons with only a slight increase in density because many of the closed voids are inaccessible to He atoms. (5) β-SiC formed from high temperature pyrolysis of a-SiC will have most of the formerly closed pores and voids opened up and rendered accessible to the outside as it undergoes close to 50% volumetric shrinkage, so its density will tend to approach that of true SiC.

Now, while the bulk density of the dry preform remains the same as before, the corresponding fiber volume fraction does not. At the state $i = -2$, the new fiber volume becomes . . .

$$f_v = f_{w,-2}\frac{\rho_{b,-2}}{\rho_f} = \frac{0.81\ \text{g/cc}}{1.95\ \text{g/cc}} \simeq 41.4\%$$

Consulting Eq(8A) from page 18 or Appendix A . . . $p_{o,i} = 1-\rho_{b,i}\rho_{m,i}^{-1} - f_v\left(1-\rho_f\rho_{m,i}^{-1}\right)$, along with the results generated in Appendices B and C, it becomes apparent that substantial changes in the complex matrix density will occur when all the helium densities are factored in. Using these new parameters, a plot of the He porosity as well as the most appropriate model function can be developed, similar to the open porosity given earlier. These results are depicted in Figure 9 below, followed by Table 10 which contains values for selected states of interest.

Figure 9. Helium porosity and model fit across the process based on He density expectations.

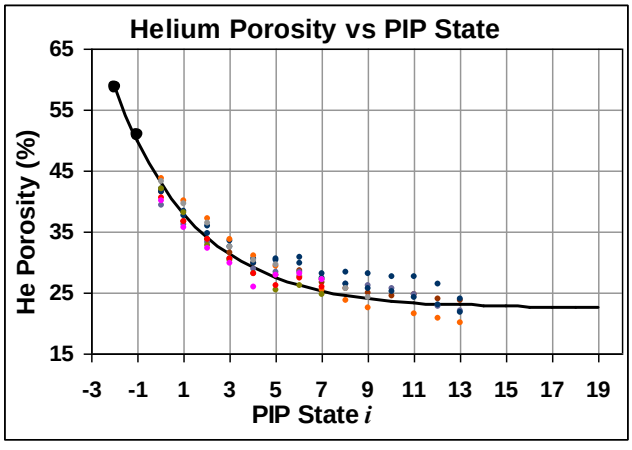

$$p_{He,i} = 20.6\, e^{-0.283i} + 22.4$$

Table 10. Selected points of interest along the C-C/SiC total porosity model curve.

Helium Porosity

Dry Preform State i = -2	Rigidization State i = -1	Carbon Pitch State i = 0	1st Ceramic State i = 1	5th Ceramic State i = 5	10th Ceramic State i = 10	13th Ceramic State i = 13	∞th Ceramic State i = ∞
58.8 %	49.8 %	43.0 %	38.0 %	27.4 %	23.7 %	23.0 %	22.4 %

At the carbon state $i = 0$, the average helium porosity fraction is indicated to be on the order $p_{He,0} = 20.6 + 22.4 = 43.0\%$, while its value after infinite densification bottoms out at a 'helium' threshold porosity of $p_{He,\infty} = 22.4\%$. Also note that at $i = 13$, $p_{He,13} = 23.0\%$ which is substantially higher than the $p_{o,13} = 13.0\%$ value already established as the average residual open porosity for fully densified C-C/SiC substrate. The difference between these two, 10%, cannot be correctly associated with the partial fraction of the total porosity that is hermetically sealed. However, it is certainly representative of the micro-porous interconnecting network that was impermeable to liquids, but more importantly . . . it includes all the voids and pores within that network which were formerly recognized as closed and inaccessible. Analogous to the true (liquid-impermeable) density defined earlier, the true He-impermeable density pertains to the fraction of material that is impermeable or impervious to gases as defined by . . . $\rho_b = (1 - p_o)\rho_t$.

Theoretical or Absolute Porosity: Properties & Speculations

The concept of theoretical (absolute) porosity bears little relevance to practical material properties but is explored here as an introspective exercise to compare with the other porosity levels and perhaps to facilitate a better understanding of the term 'total porosity'. Obviously, this would include all liquid and gas-permeable porosity subject to Darcy flow along with all the hermetically sealed voids and micro-channels which were previously impossible to breach but may be susceptible to Fickian diffusion. The absolute porosity would also include tubular pores and shielded voids in-between fiber filaments (intra-bundle porosity), porosities and certain surface morphological features within the individual fiber filaments (fiber porosity), microstructural defects, imperfections and dislocations, crystalline/lattice holes and interstitials, etc . . . In accordance with the methods applied above for the open and helium porosities, the theoretical porosity data plot shown in Figure 10 and most appropriate model values of selected interest are given in Table 11 below . . .

Figure 10. Absolute porosity and model fit across the process based on theoretical constituent densities.

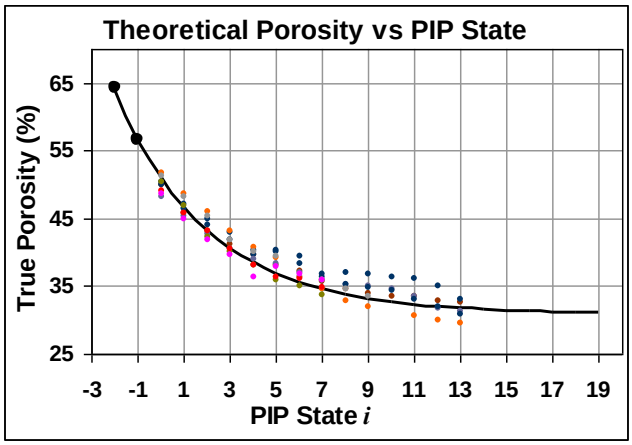

$$p_{Abs,i} = 20.2\, e^{-0.245i} + 30.9$$

Table 11. Selected points of interest along the C-C/SiC absolute porosity model curve.

Theoretical or Absolute Porosity

Dry Preform State i = -2	Rigidization State i = -1	Carbon Pitch State i = 0	1st Ceramic State i = 1	5th Ceramic State i = 5	10th Ceramic State i = 10	13th Ceramic State i = 13	∞th Ceramic State i = ∞
63.8 %	53.7 %	51.1 %	46.7 %	36.9 %	32.7 %	31.8 %	30.9 %

The potential implications from these results include a 'true' fiber volume fraction in the mid thirties (compare with the original bulk fiber volume of ~44%), a total matrix volume at i = 13 of about 33% (compare with the original matrix volume of about 43%), and a potential closed (liquid-impermeable) porosity fraction at the end of the process of ~20%! For graphical comparison, Figure 11 gives a side-by-side plot of all three porosity functions illustrating their behavior across the process.

Figure 11. Model plots of the liquid, gas and absolute porosities for C-C/SiC across the densification process

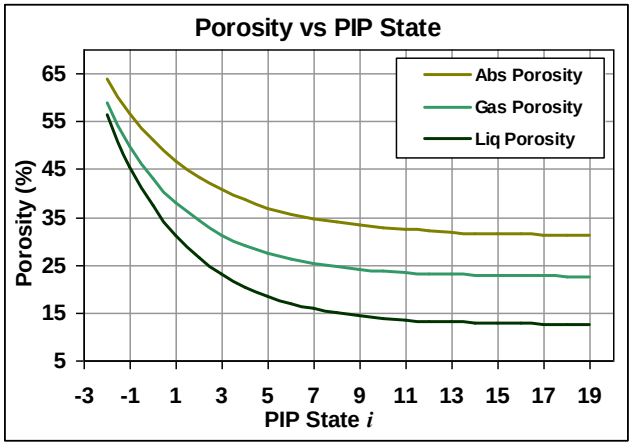

True Densities: Survey & Comparisons

Each porosity level has its own 'true' density associated with it. The 'bulk' density is simply the weight divided by the geometrical volume. It includes the total porosity of the system. The first true density excludes the liquid-permeable porosity and is impermeable to liquids, the second true density excludes the gas-permeable porosity and is impermeable to gases while the theoretical density (the absolute or perfect crystal density) is the ultimate true density of a material, in theory. This latter true density is not so practical in everyday industrial materials engineering. For comparison purposes, the four density levels of interest are plotted side-by-side in Figure 12 . . .

Figure 12. Model plots of the four levels of density relevant to the C-C/SiC system across the densification process

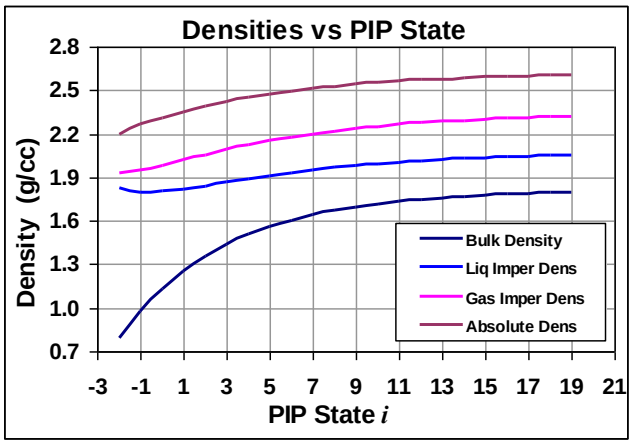

It is obvious for the C-C/SiC system, that the bulk density will never even come close to its true density (the liquid-impervious density) since both increase similarly and approach asymptotes well distanced from each other. This is in line with previous results showing that the threshold open porosity is not a small number (> 10%) – the open porosity will always represent a significant volume fraction entrenched within the material, even after many, many densification cycles are applied. Any speculations that the C-C/SiC material could be processed up into the 2.5-2.8 g/cc range or above are ambiguous. This is in accordance with the results derived earlier for Tables 8, page21 and 9, page22. It is palpable that threshold levels for both liquid and gas-permeable densities (which are unattainable in the first place) track substantially above the bulk density and are well out of the reach of physical processability.

Effects and Consequences of the Seal Coating Phase

As noted earlier from XYZ's report, the coating phase (comprised essentially of Seal Coat layers 1 thru 4) was reported to add about 0.005" thickness to the article surfaces. Again, since there is no way to confirm or refine this value, it can only be assumed that 5 mil represents that the average thickness of the combined coating layers covering the articles of interest. So how much partial volume does this add to the overall volume and how does this affect the constituent volume and

weight fractions already estimated for the substrate? It can be confirmed by examining diagrams depicting the dimensional features of the cylindrical shaft region on the pintle (between the threads and the head body), that the added coating phase of this thickness results approximately in about a 2.0% volume increase [1]. Volume changes in other regions will vary above or below this value. After the coating phase is complete, XYZ has indicated that this coating layer seals the substrate extremely well (10^{-12}-10^{-13} Darcy units) but this has not been independently confirmed. It is probably safe to assume that these layers of low-fired SiC effectively seal the ~13% porosity across most areas of the substrate, at least towards liquids. However . . . the permeability of the coating phase drastically changes once the burn cycle begins.

Thus, for the pintle shaft section, the slight increase in volume due to the applied coating phase results in a slight decrease in the fiber volume fraction to about f_v = 42.7% (compared to 43.6% for the uncoated substrate) – this scenario considers the combination of fibrous reinforcement and ceramic matrix deposited via PIP densification through cycle # 13 as the 'substrate' while the over-laid ceramic coating is a unique phase which forms a boundary or interface with the substrate surface. Likewise, an analogous decrease in the matrix weight fraction can be expected, but to get a precise delta, intricate properties of the brush-on slurry must first be estimated (including partial fractions and matrix density). Such tedious estimates will not be pursued here, rather, a few descriptive attributes will just be highlighted.

These types of brush-on slurries generally contain 30-50% particles by weight in resin (about 40% fine β-SiC particles are slowly blended into liquid SMP-10 resin). The viscosity of SMP-10 polymer resin is low enough so that solvents are usually not required in order to make latex-consistent, paintable slurries (if needed however, typical solvents for SMP-10 include toluene, THF, hexane and naphtha). The content of the primary surfactant (a leveling/wetting agent) in the slurry mixture is relatively small (on the order of 1-3%) – it could conceivably be omitted in rough calculations involving partial fractions, if desired. However, the volume fraction of entrained air is not negligible. Entrained air is generated during mixing and application of the slurry and much of it is retained in the fired coating overlay . . . For these types of slurries, without the application of vacuum or pressurized curing, entrained voids and porosity are not only inevitable, they are unavoidable.

Thus, as it was with the porous substrate, the brush-on coating phase will have both a bulk density and a true density associated with it. Micro-pockets of entrained air comprise the porosity fraction of the coating phase . . . a substantial fraction of these pores are isolated and completely nonconnected, and many being these are hermetically sealed. In a nutshell, the brush-on phase can be described as a composite coating overlay consisting of β-SiC particles and entrained air (porosity, voids and bubbles) embedded in a glassy matrix of a-SiC.

It is well substantiated by now that vacuum-forced impregnations of low viscosity SMP-10 liquid into the surface porosity of the substrate achieve much better mechanical bonding effects within and across the substrate than high viscosity particulate slurries which are loosely applied with no forced augmentation. The data and post-fire results for some of the HT tests clearly indicate this

[1] "Orion Launch Abort System (LAS) Attitude Control Motor (ACM) High Thrust Test No. 7 (HT-7) Static Test Readiness Review (TRR)", March 27,2008

condition. Furthermore, the boundary interface between the vacuum-impregnated substrate and the first brush-on layer (Seal Coat #1) appears to be the weakest interface in the entire C-C/SiC system. This built-in weakness, in combination with the ~50% reduction in volume that occurs as surface-bound a-SiC is transformed into β-SiC during the firing cycle, raises serious concerns regarding the viability of the current C-C/SiC (manufacturing) concept being proposed by FMI (the manufacturing approach, not the material concept).

While there are certainly other problem areas associated with the current C-C/SiC approach, this single aspect, the method for coating and sealing the substrate, would need to be addressed first. Specifically, brush-on slurries, as convenient, expeditious and cost effective as they may seem to be, inevitably produce weak interfaces and should be phased out of this kind of system, even if cost and time factors are increased. These weak interfaces are potentially catastrophic and cannot be compensated for by applying additional layers of material on top of the layer that is already loosely bound. More importantly, this approach can never compete with layers that are mechanically forced into and onto the substrate with PIP-type vacuum/pressure effects (which provides a hint as to how these layers might be applied).

Too often however, statements such as these become misconstrued by many who inevitably conclude that C/C and CMC materials are inadequate for these types of applications. On the contrary, there is a long history of successes using a variety of C/C and CMC material systems whose manufacturing process has been well optimized to meet the conditions of the particular application at hand. Unfortunately, a small number of these trials met their demise because of a minor, inadvertent or unreported process change, or because a single manufacturing step, which could have been modified, supplemented or eliminated, caused an otherwise highly superior material system to appear inferior, and rather than taking the actions to eliminate these minor anomalies, the stakeholders abandoned the material concept altogether.

As a supplement to the foregoing discussions, strategies using these tools can be improvised for other material systems by optimizing or refining the concepts of density, porosity and partial fractions specifically for these platforms. Much of the methodology developed in the previous sections (and the Appendix sections) can be applied to ordinary and advanced composite systems such as the carbon cloth phenolic (CCP) structures which are used as the primary ablative material in RSRM flame-side aft exit cone (nozzle) sections. It is beneficial to already understand some of the tools presented in earlier sections in order to fully appreciate their applications in the following sections.

During the Ply Lifting Technical Interchange Meeting held in March 2006, a consortium of companies and participants presented a variety of data, and one of the more interesting charts included physical measurements of open porosity and helium porosity (liquid-permeable and gas-permeable porosities) at various temperatures for CCP nozzle material. Figure 13 replicates this chart [1] which depicts open porosity, helium porosity and mercury porosimetry data taken for FM5055 CCP test samples subjected to several temperatures up to the point where pyrolytic conversion of the material is essentially complete. While there is not much data to consider, a best effort approach will be pursued.

Figure 13. Measured porosity data for CCP test samples processed at various temperatures.

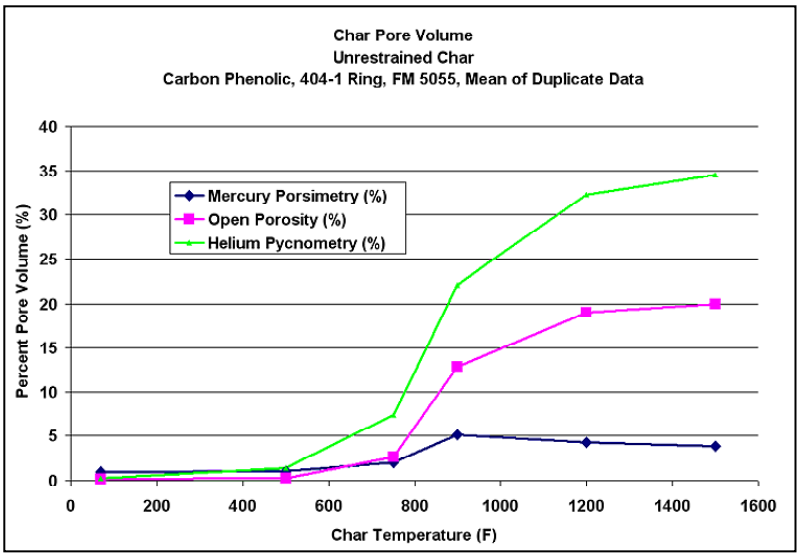

As indicated earlier in the introduction section, mercury porosimetry not only damages the internal structure of the sample in C-C/CMC materials but provides unacceptable quantitative results. This is obvious in Figure 9. Additionally, pore radii and size distributions produced by this method should be highly scrutinized. Thus, the Hg porosimetry data given here will not be included in the analysis . . . However, further evaluation of the data points describing the behavior of the open and helium porosities over temperature appear to be very relevant. These curves can be utilized to provide some very interesting insight in terms of the density, porosity and constituent fractions as the CCP material responds to pyrolytic conversion from a general point of view.

[1] "Ply Lift TIM – Theory Discussion", presented by Dave Richardson, March 7-8, 2006

To obtain this data, the test operator probably pyrolyzed samples of FM5055 CCP material to various temperatures, let them cool down passively to ambient and then conducted the porosity tests. In all likelihood, these results cannot accurately represent porosity development under the unusual conditions of rapid or excessive heating rates, such as those comparable to real life nozzle environments. However, for purposes of introspection, this data might conceivably be treated as an irreversible quasi-static process roughly tracking the evolution of porosity in the composite as the temperature is incrementally raised from ambient conditions through the pyrolysis process.

In contrast to the preceding C-C/SiC discussions involving multiple pyrolysis (and impregnation) cycles across a controlled incremental densification/manufacturing process, the current case is more reflective of one of the (single) pyrolysis cycles where the porosity is plotted over temperature. Here, instead of monitoring composite properties as they statically change along a dimensionless process line, their change is dynamically examined as a function of applied temperature as the material is converted from the as-molded PMC state to the fully carbonized (C/C) state. Similarly however, only the matrix phase undergoes thermal conversion while the (already carbonized) fibrous reinforcement remains unchanged . . . that is, until the material temperature reaches the maximum process temperature previously applied to the fiber/fabric product during its manufacturing process. Then, a different phenomenon takes over.

CCP Porosity: Functional Characterization & Estimations

The data in Figure 13 can be treated in a similar fashion as that which was done in the foregoing C-C/SiC discussions by re-plotting the values and modeling the curves with the most appropriate function precisely describing the upper and lower extremes along with the data points in between. This approach is depicted in Figure 14 below . . .

Figure 14. Re-plot of the porosity values given in Figure 9 along with the most appropriate model fits.

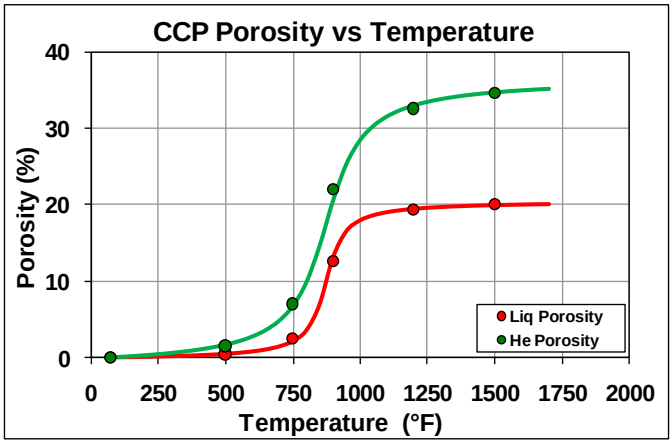

In contrast to the single asymptote, reverse exponential-type response function again, was most fitting for densification processes, the data in Figure13 was found to be best represented by a double asymptotic reverse trigonometric function of the form . . .

$$P = a\left[1 - ArcTan\left(-bx + c\right)\right] + d$$

Rather than utilizing the natural asymptotic boundaries called out by this function [1], the upper and lower limits are driven by the data which implies a lower boundary of zero porosity at room temperature ($T_0 \sim 75°F$) and a maximum porosity threshold p_t that appears to reach a plateau around 1600°-1700°F. The porosity threshold is found to be a function of the coefficients a and d, such that . . . $p_t = 2(a + d)$. Now as $x \rightarrow T_0$, $a\left[1 - ArcTan\left(-bT_0 + c\right)\right] + d \rightarrow 0$ and . . . $a = \frac{1}{2}\, p_t \Big/ ArcTan(-bT_0 + c)$. Specific functions describing the open (liquid-permeable) porosity and helium (gas-permeable) porosity data depicted in Figures 13 and 14 were found to be . . .

Open (Liquid-Permeable) Porosity

$$p_o = 6.62\left[1 - ArcTan\left(-0.02T + 17.5\right)\right] + 3.36$$

Helium (Gas-Permeable) Porosity

$$p_{He} = 12.12\left[1 - ArcTan\left(-0.01T + 8.75\right)\right] + 5.41$$

which gives maximum porosity thresholds at 1600°F of $p_{o,t} = 2 \times (6.62 + 3.36) = 20.0\%$ and $p_{He,t} = 2 \times (12.12 + 5.41) = 35.1\%$ respectively. The porosity change appears to level off at a threshold temperature of $T_t = 1600°F$, but this is not necessarily the same threshold temperature that pertains to the end of matrix char conversion (the threshold temperature corresponding to 100% char conversion has been determined to be around 1100°-1200° when subjected slow pyrolysis). It was also found that the other two coefficients appeared to be related, that is . . . $c_o = \frac{1}{2}\, c_{He}$ and $d_o = \frac{1}{2}\, d_{He}$, which seems to comply with the expectation that the two porosity curves be 'in phase'. It is obvious that the particular functional type selected for this analysis provides an excellent fit to the raw data and complies exceptionally well with the limitations of the boundaries.

As noted earlier, independent studies have substantiated that slow, non-ablative pyrolysis of as-molded phenolic articles typically results in about a 1-2% thickness decrease in the out-of-plane direction due to interlaminar matrix consolidation as it undergoes carbonization from the organic state to inorganic glassy char. This interlaminar shrinkage effect is substantially lower for articles cured under excessive pressures (> 100 psi) such as some of the current carbon cloth phenolic (CCP) systems. A precise approach accounting for fiber volume changes might include this minor volumetric decrease, but for the rough estimations developed here, it can be ignored. Additionally, it is well understood that a substantial fraction of the raw composite volume is eroded away during a typical nozzle burn process. Since material losses due to erosion for each of the three constituents comprising the CCP system are almost certainly *not* identical, the erosion process is expected to exhibit a certain degree of anisotropy, depending on the localized volume distributions of fiber, matrix and carbon black powder encountered by the degradation plane as it moves throughout the material.

However, for this analysis, erosion anisotropies will be ignored so that the loss of bulk composite volume due to erosion produces no significant change in the effective volume *fractions* for each of the constituents. This is analogous to an article which is machined in half – while the net volume for each is only half the original volume, the constituent volume fractions all remain

[1] Please recall or review the functional techniques developed and applied to the C-C/SiC system earlier.

unchanged. On the other hand, since the charring/carbonization portion of the burn process produces a net change in the matrix phase, the relative constituent fractions also change in accordance with the matrix change. All in all however, these conditions permit simplification through direct analogies with previous discussions in the report, particularly the Appendices, regarding the almost-invariant nature of fiber volume fractions during pyrolytic conversion.

CCP Matrix Content: Functional Characterization & Estimations

Most of the constituent data readily available nowadays for Reusable Solid Rocket Motor (RSRM) CCP composites is derived from NARC-based MX4926 material. While FM5055 may have been based on the older American Enka or Avtex reinforcement (circa 1970's-1990's), CCP composites identically fabricated from any of these materials are probably similar enough to be represented approximately by the porosity data given in Figures 13 and 14, on the average. Some of the nominal property values relevant to this analysis are given in Table 12, followed by sources and justifications for these numbers . . .

Table 12. Nominal and average property values for NARC MX4926 CCP and constituent materials.

Average As-Molded NARC MX-4926 Constituent Data

Matrix/Resin Weight Fraction [1]	Carbon Black Weight Fraction [1]	Fiber/Fabric Weight Fraction [1]	Cured Bulk Composite Density [1]	NARC Rayon Bulk Fiber Density [2]	Carbon Black Bulk Particle Density [3]	Cured SC1008 Phenolic Resin Density [4]	Pyrolyzed SC1008 Resin Density [4]	SC1008 Resin Char Yield [4]
34.5 %	15.3 %	50.2 %	1.50 g/cc	1.81 g/cc	1.35 g/cc	1.24 g/cc	1.45 g/cc	56.0 %

1 - Average values extracted from "Phase I. Screening and Down-Selection of Rayon Replacement Materials (NSP Carbonized Materials)", ATK Aug, 2001. Resin content, carbon black content and bulk composite density were averaged from Table A, Cytec Fiberite data which they acquired using test procedure, STW5-3279, "Material Specification for Carbon Cloth Phenolic, Preimpregnated". Fiber content was deduced from the measured values of resin content r_w and carbon black content $c_{b,w}$, . . . $f_w = 1 - r_w - c_{b,w}$ to give a normalized total for the three constituents.

2 - Average value extracted from "Phase I. Screening and Down-Selection of Rayon Replacement Materials (NSP Carbonized Materials)", ATK Aug, 2001. In this study, fiber densities were obtained via the ASTM-1505 Density Gradient Technique, an Archimedes/buoyancy method which means this is the liquid-permeable (bulk) fiber density. Analogous to the HS40 PAN fiber examined earlier during the C-C/SiC discussion, the average gas-permeable (helium) density for this particular NARC fiber is expected to be around 1.90-1.91 g/cc.

3 - The majority of particle densities reported in the literature for carbon black appear to reference the true (gas-impermeable) density which runs in the range 1.86-1.9 g/cc. However, relative to matrix resins and non-volatile composite constituents, its bulk (liquid-permeable) density is expected to be comparable to that of carbonized pitch residues discussed earlier and provided in Table 1 [1].

4 – Independent characterization of Borden's SC1008HS phenolic resol resin before and after pyrolysis has been quite extensive with over 500 density/porosity tests personally conducted on resin samples cured under pressure and then carbonized to a variety of temperatures from 1000°-1800°F. The values presented in this table represent the average of all those tests. Also, char yields for SC1008 have been characterized independently close to 200 times. 56.0% is considered to be the average threshold char yield after 100% conversion on samples subjected to slow pyrolysis (>8 hours duration). Due to a very low level of micro-porosity in pressure-cured phenolic resins, the liquid-permeable and impermeable densities are almost equivalent. After pyrolysis however, the charred remnant contains close to 40% void space. Some of these are closed, non-interconnected micro-voids and about a third overall are hermetic sealed to gases [1], preventing the glassy char from ever approaching the theoretical (graphite) density.

[1] "Development of Anode Binder Pitch Laboratory Characterization Methods", E. R. Mchery, J. T. Baron and K. C. Krupinski, Koppers Industries Inc, Pittsburgh, PA

Techniques developed for the porosity can be applied to other properties, such as those pertaining to the matrix and to composite densities. It should be realized however, that changes in the matrix content do not necessarily track precisely along with the porosity curve at all points. This is apparent at the lower temperatures where early increases in porosity are expected, due to swelling and expansion effects. On the other hand, *matrix and density changes occur strictly as a result of thermal conversion of the polymer matrix into the higher density glassy carbon char* (i.e... 1.24 g/cc $\rightarrow$ 1.45 g/cc). As isolated, non-interacting entities, the fiber and the matrix may expand and contract freely, without restraint and without hysteresis. However, in a combined composite system, inner stresses are established, particularly along fiber-matrix interfaces, as *the constituents tend to restrain each other* to varying degrees during heating/cooling ramps. Presumably, the raw porosity test samples were heat treated, cooled down and then tested. Upon cooling, residual effects may include hysteretic volume changes in some of the pores and voids immediately surrounding the fiber interfaces and at bundle intersections, possibly leading to a slight increase in apparent porosity in cooled samples. These properties can also be substantially influenced by relative CTE effects as the cured virgin phenolic resin (α ~ 70-80 X 10^{-6}/ppm)[2] is converted into glassy carbon char (α ~ 3-4 X 10^{-6}/ppm)[2].

During slow pyrolysis, independent testing has revealed that these types of cured phenolic resins just begin to undergo thermal degradation in the 550°-650°F range and are fully carbonized before about 1100°-1200°. When pyrolysis of a CCP composite is 100% complete, the polymer matrix is completely converted into glassy char. The raw weight of carbonized polymer in the system w_{cp} is derived simply by the effect of the threshold char yield y_t on the original resin weight w_r, that is . . . $w_{cp} = y_t w_r$. In accordance with the principles developed in Appendix A[3], the carbonized (glassy) polymer content $c_{p,w}$ (its fractional weight percentage out of the total composite weight) is also determined by the effect of y_t on the resin content r_w, that is . . .

$$c_{p,w} = w_{cb}\left(w_f + w_{cb} + w_{cp}\right)^{-1} = y_t r_w\left(f_w + c_{b,w} + y_t r_w\right)^{-1}$$

where w_f, w_{cb}, f_w and $c_{b,w}$ are respectively, the raw weight of fiber, the raw weight of carbon black, the fiber weight fraction and the carbon black weight fraction. Using the values given in Table 12, the average charred polymer content after 100% pyrolytic conversion comes out to be . . . $\boldsymbol{c_{p,w} = 22.8\%}$. With similar techniques as those applied to the porosity data above, the total matrix fraction as a function of temperature can be generated. These results are given in Figure 15 on page 35 . . .

[1] "The Effects of Particle Size on Small Angle Neutron Scattering From a Granular Phenolic Resin Char",J.M. Caloand P.J. Hall, Dept. Chem. Eng, Brown University.
[2] Reference data from SPI Vitreous Carbon Products, Tokai Glassy Carbon Products USA and MatWebMaterial Property Database from proprietary sources.
[3] Please consult Appendix A for techniques, formulas, derivations, constituent relationships and definitions pertaining to the subscript notations used in this study.

Figure 15. Curve trace and model fit for CCP material over temperature.

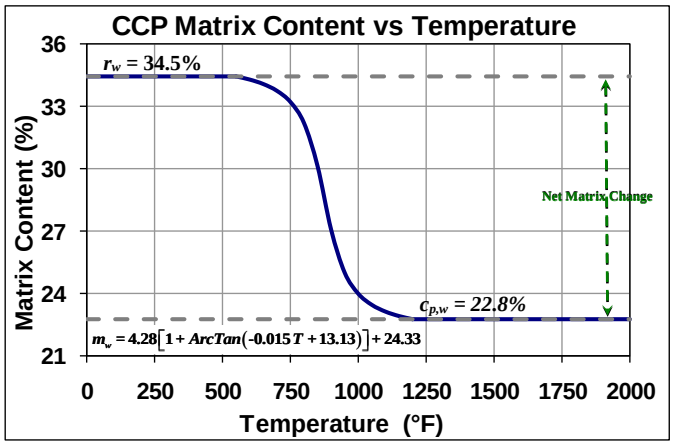

In contrast to the porosity functions, the decreasing matrix content takes an analogous form . . . $P = a\left[1 + ArcTan\left(-bx + c\right)\right] + d$, where r_w (the initial resin content) and $c_{p,w}$ (the final carbon char content) are related, that is . . . $r_w + c_{p,w} = 2(a + d)$ or $d = ½\,(r_w + c_{p,w}) - a$. Defining the temperature at which matrix carbonization begins, $T_0 \sim 550°\text{-}600°\text{F}$ and the (threshold) temperature corresponding to 100% char conversion, $T_t \sim 1150°\text{-}1200°$, it is obvious that as $x \rightarrow T_0$, $a\left[1 + ArcTan\left(-bT_0 + c\right)\right] + d \rightarrow r_w$, giving . . . $a = ½\,(r_w - c_{p,w}) \,/\, ArcTan(-bT_0 + c)$ which emphasizes the upper boundary or pre-char plateau region. On the other side, as $x \rightarrow T_t$, $a\left[1 + ArcTan\left(-bT_t + c\right)\right] + d \rightarrow c_{p,w}$, which gives an alternate value for a , namely . . . $a = ½\,(c_{p,w} - r_w) \,/\, ArcTan(-bT_t + c)$ emphasizing the lower boundary post-char region. In either case, the parameters b and c become defined as multiples of the coefficients identified for the original porosity curves in order to maintain in-phase synchronicity throughout. Thus, as given in Figure 15, the total matrix content can be represented most appropriately by . . .

$$m_w = 4.28\left[1 + ArcTan\left(-0.015\,T + 13.13\right)\right] + 24.33$$

. . . from which $2 \times (4.28 + 24.33) = r_w + c_{p,w} = 34.5 + 22.8 = 57.2$. Of course, this represents the total matrix phase which consists of varying levels of virgin phenolic resin and charred resin. To be thorough however, in addition to virgin resin and 100% carbon char, this complex matrix encompasses almost an infinite number of intermediate and transitional forms, comprised of partially converted products across a 'gradient conversion char zone' separating virgin thermoset resin from fully charred glassy carbon. It would be an impossible task to try and identify all of these species, but it is fallacious to simply divide the system into virgin polymer and fully converted char. For the limited scope of this discussion however, it would still be insightful to at least examine a simplified or generalized approach. This may be feasible by taking to mind the concept of partial fractions[1].

Representative partial fractions of unadulterated virgin resin and non-virgin resin in various degrees of carbonization can be surmised for these two 'phases' by applying techniques similar to those used above . The results are depicted in Figure 16 . . .

[1] Please consult Appendices B-C for techniques, derivations and estimation concepts regarding the relevance of partial fractions in composite systems.

Figure 16. Representative curve traces for virgin and charred phenolic matrix in CCP material over temperature.

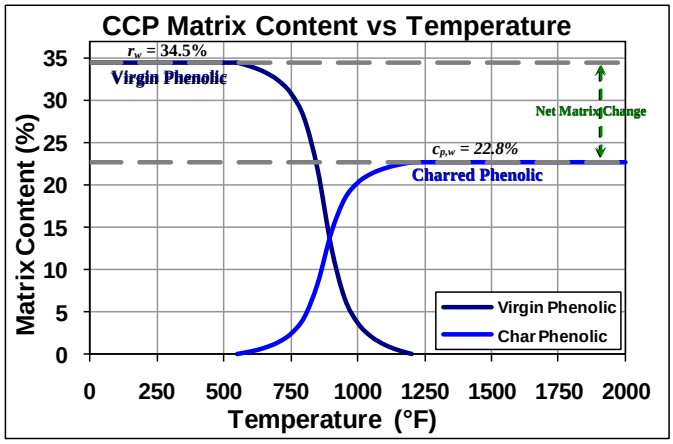

Using the same functional techniques as those applied above, the initial virgin resin content and final (threshold) char content are defined respectively by . . . $r_w = 2(a + d)$ and $c_{p,w} = 2(a + d)$. Then, in each case as x goes to T_0 and T_t, the values for the coefficient a can subsequently be defined for each matrix fraction at the lower boundaries, $a_r = ½\ r_w \,/\, ArcTan(-bT_0 + c)$ and $a_c = ½\ c_{p,w} \,/\, ArcTan(-bT_0 + c)$, and then at the upper boundaries, $a_r = -½\ r_w \,/\, ArcTan(-bT_t + c)$, and $a_c = -½\ c_{p,w} \,/\, ArcTan(-bT_t + c)$ to give the respective functional results for the decreasing virgin matrix content and the increasing non-virgin matrix content respectively, that is . . .

Virgin Matrix (Resin) Content

$$r_w = 12.59\left[1 + ArcTan\left(-0.015T + 13.13\right)\right] + 4.64$$

Non-Virgin Matrix (Char) Content

$$c_{p,w} = 8.31\left[1 - ArcTan\left(-0.015T + 13.13\right)\right] + 3.07$$

. . . where $r_w = 2$ X (12.59 + 4.64) = 34.5% and $c_{p,w} = 2$ X (8.31 + 3.06) = 22.8% accordingly.

Obviously, the precision in accuracy here is unsubstantiated and these results may be more illustrative than quantitative. However, the implied microstructural and compositional transition region between virgin and charred polymer (~550°–1200°F) exhibits a unique resemblance to other bimaterial systems studied in which the transition/conversion phase has been characterized via EDX and X-Ray diffraction techniques (namely, multiphase ceramic matrix and C/C composite systems). Thus, now it is possible to deduce a complete data table of partial fractions across the entire temperature range containing estimated values for the fiber weight fraction (fiber content) f_w, the carbon black content $c_{b,w}$, the virgin resin content r_w, and the charred polymer content $c_{p,w}$. Selected points derived from these efforts are given in Table 13 below. Also, using the following formula to estimate bulk densities and 'true' densities [1], representative values for the CCP bulk density, liquid-impervious density and helium density as functions of temperature can be tabulated and plotted across the charring/carbonization process. These results are given in Figure 13 below . . .

$$\rho_b = \left(f_w\rho_f^{-1} + c_{b,w}\rho_{cb}^{-1} + r_w\rho_r^{-1} + c_{p,w}\rho_{cp}^{-1}\right)^{-1}\left(1-p\right) = \rho_t\left(1-p\right)$$

[1] Reference formulas 4A and 5A in Appendix A at the end of the report.

Table 13. Partial fraction estimates and physical properties for CCP material undergoing pyrolytic conversion.

Pyrolytic Physical Properties for NARC MX-4926

T Pyro Temp (°F)	f_w Fiber Content (%)	$c_{b,w}$ Black Content (%)	r_w Resin Content (%)	$c_{p,w}$ Char Content (%)	p_o Open Porosity (%)	p_{He} He Porosity (%)	ρ_b Bulk Density (g/cc)	ρ_t True Density (g/cc)	ρ_{He} He Density (g/cc)
550°	50.2	15.3	34.5	0.0	0.6	2.1	1.49	1.50	1.52
600°	50.3	15.3	34.0	0.3	0.8	2.7	1.49	1.50	1.53
700°	50.8	15.5	32.4	1.3	1.4	4.8	1.48	1.50	1.55
800°	52.0	15.8	27.9	4.4	3.5	9.7	1.46	1.52	1.62
900°	55.9	17.0	12.7	14.4	13.0	20.5	1.37	1.57	1.72
1000°	59.3	17.7	3.6	20.4	17.9	28.4	1.32	1.61	1.84
1100°	58.9	17.9	1.1	22.0	18.9	31.5	1.31	1.61	1.91
1200°	59.2	18.0	0.0	22.8	19.4	32.9	1.31	1.62	1.95

Figure 17. Bulk density, liquid-impervious (so-called 'true') density and helium density for CCP material undergoing pyrolysis.

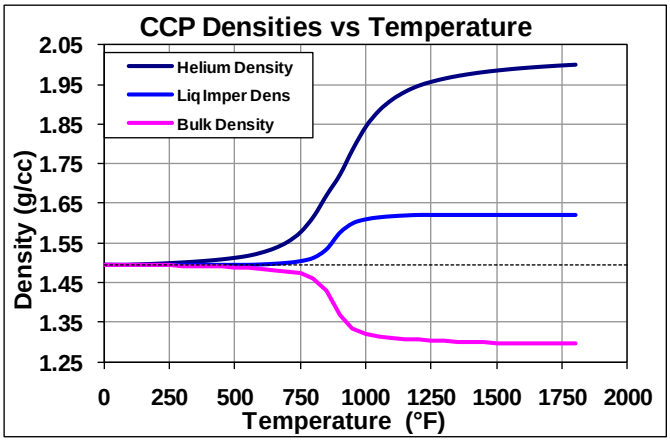

Thus, the liquid-impervious density is the 'true' density relative to the bulk density in terms of the material's permeability towards liquids while the helium density (or gas-impervious density) is the 'true' density relative to gas permeability. Note that the bulk density decreases throughout the pyrolysis process in accordance with and indirectly proportional to the porosity that is created. True densities reflect the skeletal (non-porous) volume of the composite, that is, the solid fiber/resin/black combination (i.e... the bulk volume minus the porosity fraction). Consequently, as the internal volume of the composite becomes more porous, the skeletal volume becomes more dense. Thus, even though the net matrix weight fraction decreases throughout the pyrolysis process, the true densities increase as they diverge from the original density because the matrix density increases as it is converted from organic polymer thermoset into glassy vitreous carbon. Obviously, these curve traces could be modeled in the same functional manner as the other properties, is so desired.

Now, re-examine Figures 14, 15 and 16 and note that the inflection point along each of these functional curves is indicative of the mid-point in the process, corresponding to an estimated inflection temperature of $\boldsymbol{T_I}$ **= 875°F**. This is surmised by use of the second derivative [1]. Also note that the inflection point represents the *maximum conversion ratio* for the given property in terms of pyrolysis temperature by use of the first derivative, as outlined in Appendix E. These inflection values can then be evaluated for any of the properties examined so far as provided in Table 14 . . .

Table 14. Maximum (inflection) pyrolysis conversion ratios for a few CCP properties and constituents.

Maximum Conversion Ratios for CCP Properties

Inflection Temperature	Open Porosity	Helium Porosity	Total Matrix	Virgin Matrix	Non-Virgin Matrix
875°F	13.2 %	12.1 %	-6.4 %	-18.9 %	12.5 %

Note that the open and helium porosity creation rates are not exactly identical while the net (total) matrix change is equal to the sum of the partials. However, these results should not be interpreted with too much significance. Given the non-dynamic nature of the sampling and testing procedures used for measuring the original porosity data, it is questionable how well these conversion ratios or rates can actually reflect instantaneous property changes for any given real-life scenario, or if they can at all. It is not too likely that these results will provide any meaningful insight relative to rapid heating ramps. They are perhaps more representative of pseudo steady-state conditions with quasi-static connotations and are given here primarily for academic purposes.

However, another piece of data that proved to be interesting was also provided in the study, "Phase I. Screening and Down-Selection of Rayon Replacement Materials (NSP Carbonized Materials)", ATK Aug, 2001, as given in Table X, “Thiokol Panel Test Results”. Thiokol’s test results in this table for the NARC control material included (1) DSC onset temperature of 410°F, (2) TGA weight loss at 662° of 1.45%, (3) TGA weight loss at 1292° of 14.84% and (4) TGA weight loss at 1652°F of 16.26 %. In contrast to the previous analysis, this data was generated instantaneously as the dynamic TGA test procedure was carried out at an unknown heating rate. In all likelihood however, this heating rate was rather high, perhaps a hundred degrees per minute, since the companies conducting these tests back in this era (Thiokol/SRI) were already experimenting with rates in the 1000’s. Uncorrected, rates of this order produce grave differences in data gathered at the slower, conventional quasi-static TGA test rates. Significant thermal lags and induction periods are heavily controlled by instantaneous conductivity effects, sometimes causing pyrolysis temperatures to appear higher than those obtained at the slow heating rates. Obviously, the low rates allow the material to absorb energy and respond by completing the expected chemical reaction sequences whereas during rapid heating, these processes tend to overlap. While the DSC onset temperature is not directly tied to weight change data, the implication is that the beginning of the energy releasing reactions corresponds to the generation of pyrolysis gases (or post-cure volatiles) and hence weight losses. This data is expected to exhibit higher inflection and threshold temperatures than the static cases evaluated earlier.

[1] Reference formula 2E in Appendix E and the surrounding discussion for elaboration of these techniques.

Using formula (3E) in Appendix E, the char yield uniquely associated with this data set comes out to be y_t = 56.2%. This is considered as the threshold char yield and the carbonization/conversion process is presumed to be 100% complete before 1600° (even under uncorrected rapid heating rate conditions). Also, using Eq(4E) developed in Appendix E[1], the degree of conversion can be estimated directly from the pyrolysis weight loss data, and a model fit can be attempted by setting the 100% conversion plateau equal to 2(a + d), as done before. These results are summarized in Table 15 and illustrated Figure 18 below . . .

Table 15. TGA weight loss data and estimated conversion rates for NARC control material.

Pyrolysis Weight Loss Data for NARC

TGA/DSC Test Temperature	TGA (Pyrolysis) Weight Loss	Degree of Pyrolytic Conversion
410°F	0.0 %	0.0 %
662°F	1.5 %	8.9 %
1292°F	14.8 %	91.3 %
1652°F	16.3 %	100.0 %

Figure 18. Fractional conversion of NARC material undergoing high speed TGA pyrolysis.

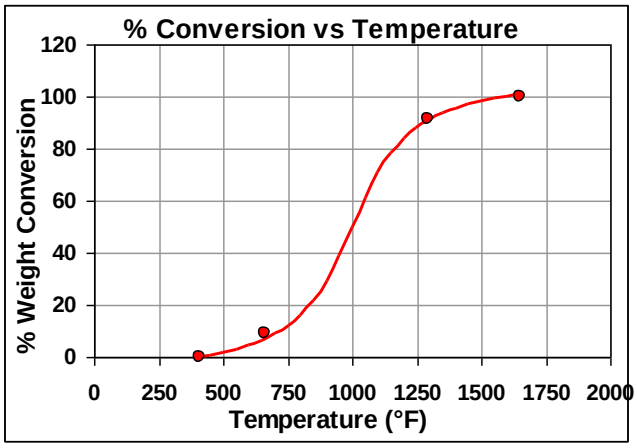

Obviously, this is not really enough data to do a realistic characterization or draw an abundance of conclusions from, so a 'best effort' approach has been attempted (with caution) in order to perceive any possible insight which may be available from the data. Using techniques similar to those developed for previous examples, the 'best fit' functional representation of this data gives . . .

$$\%C \;=\; 38.6\left[1-ArcTan\left(-0.006\;T+6.0\right)\right] \;+\; 11.4$$

. . . where 2 X (38.6 + 11.4) = 100% which corresponds to a threshold conversion temperature of $T_t \simeq$ 1590°F. Additionally, the inflection temperature for this data [1] comes out to be T_I = 1000° corresponding to a maximum conversion rate of k_I = 23.1% / °F in net composite weight at the midpoint of the pyrolytic conversion process. This is quite reflective of the relatively high heating rate that must have been used in Thiokol's TGA test.

[1] Please consult formulas 3E and 4E in Appendix E and the surrounding discussion for estimation methodolgy of conversion rates.

Final Comments and Speculations Associated With CCP Phenomena

A last glance at the original porosity data calls to mind a couple of interesting points. As the matrix passes through pyrolysis and the temperature continues to rise a new functional description or model must take over because, at some point, the structure and properties of the low-fired rayon reinforcement will begin to change. Of course, if the system ever got up to a level > ~ 5000°F, the glassy carbon phase itself may attempt to crystallize or thermally degrade. Thus, the porosity data given in Figure 13, page 30 and the analysis thereafter is only valid until somewhere in the 2100-2600°F range when the fiber phase itself begins to undergo significant changes . . . particularly, changes within the fiber-matrix interphase region related to fiber microstructual consolidation and re-orientation, fiber/bundle volumetric and diameter reductions, changes in fiber surface morphology and topology, and changes in interphase chemistry or specifically, the destruction of surface coupling groups joining the fiber and matrix phases. There is also a possibility that the adverse effects associated with the use of 'green' rayon reinforcements used in current CCP materials might have some bearing on late-term ply lifting events. In any case, the present study has focused strictly on pyrolytic composite changes occurring prior to about 2000°. The second point alluded to above will be expounded on later.

Current theories of ply lifting in CCP materials rest heavily of factors associated with the pressure build-up of volatiles in closed pores (or pores with very narrow escape paths) as the material progresses through the burn cycle. Such drastic increases in gas-permeable porosity at higher temperatures, as depicted in Figure 13, page 30, tend to make one wonder how 'pore pressure' could ever play a major role in phenomena such as ply lifting. However, viscous tar-like exudates produced during *rapid* pyrolysis (or firing) of phenolic materials probably have great difficulty flowing through the gas-permeable micro-pores. While these pore channels will effectively accommodate the escape of pyrolysis gases, many may be closed off by the thick exudate as it seals over and blocks the smaller pore openings, potentially facilitating marked increases in internal pore pressure.

Independent studies have confirmed that phenolic resins retain a small degree of plasticity after attaining maximum cure temperature and do not reach full brittle hardness until they are cooled down from the curing process [1]. So how could such levels of liquid exudate be generated in a hardened thermoset matrix upon re-heating? Most of the cured phenolic matrix medium consists of highly cross-linked networks which exhibit minimal T_g effects upon re-heating and then begin to transform into glassy carbon above about 550°-600°F – *in the solid state*. However, the bulk macro-structure will inevitably contain regions of lower crosslink density which did not cure as completely as other areas in the matrix body and which may be surrounded or shielded by material which is more hardened and crosslinked. These softer regions will tend to exhibit thermoplastic behavior to varying degrees upon re-heating, passing through a marked T_g zone and then attempting to flow out of the region as they enter a semi-melting phase. Large macro-pores which comprise the bulk of the 'open' porosity are generally permeable to thick liquids, including viscous resins and tars (under high temperatures, these semi-liquids are readily driven through the macro-porous channels).

[1] Reference item number 4 on page 33.

At some point, it is likely these semi-mobile, low crosslink density regions will begin to undergo rapid thermal crosslinking due to advanced post-curing effects and pyrolytic conversion mechanisms (and the mobile phase may encounter more reactive crosslink sites as it migrates out of the local area). Additionally, when there are no phenol groups available for normal bond formation, *pyrolytic crosslinking* may begin to take place. Advanced crosslinking between methylene carbon centers and available ring positions is one of the primary mechanisms associated with the pyrolytic conversion of thermoset polymers, ultimately leading to the final glassy structure. Potentially, these advanced reactions could produce localized viscosity-increasing effects, perhaps causing the tar to become more like a thermoset. At pyrolysis temperatures, unless the exudate is physically forced out of the material somehow, it must either degrade and volatilize or carbonize via advanced crosslinking.

As with most composite resins, uncured phenolic resins are solutions . . . solutions of monomers (phenol, formadehyde, cresols, resorcinols), dimers, trimers, staging intermediates and oligomers (substituted methylol phenols, polymethylene-linked polyphenols, and an analogous array of polysubstituted ethers), solvent (typically IPA), residual and latent water (condensation water and residual moisture are expelled and re-generated throughout the entire thermal history of resols and novolacs from the low viscosity Stage A resinous state through the hardened C Stage and much of the solid state pyrolysis process). When heat and vacuum are applied to an uncured liquid resin embedded in a fibrous medium (i.e... a prepreg lay-up), the constituent resin molecules travel at different speeds across the fiber surfaces (much like a chromatography separation process). Differential molecular migrations eventually lead to greater separation distances between resin components as some tend to become partitioned in the mobile (resin) phase and others in the stationary (fiber) phase. These motions are driven by the absorbed heat and the autoclave vacuum forces as the mixture of resin components is compelled to flow towards the periphery of the composite while the staging process carries the resin closer to its gel point. Not surprisingly, along with solvent and water, the monomeric reactants formadehyde and then phenol are some of the first molecules to leave the system.

Sometimes, specific regions identified as ‘resin-starved’ or those appearing to exhibit low resin content after cure are actually areas in which the solution mixture has gotten out-of-balance during the staging and/or curing process. Incorrect staging procedures are particularly notorious for contributing to distribution/formulation variations – before the prepreg is ever exposed to the final curing process (some fabricators do not always fully understand the science or ramifications of user-applied staging strategies and would be better off to let the prepreg manufacturer stage the material for them). In any case, after the cure process, there will be domains with fewer crosslinks than the surrounding regions as distributions in resin content, composition and degree-of-cure tend to vary from one location to the next. In many cases, these softer regions are *not* resin-starved but are starved of the reactants necessary to effectively complete the crosslinking process to its full extent.

Resin distributions are also influenced by the specific lay-up/bagging configurations and autoclave curing profiles applied. Optimally staged prepreg material will tend to minimize abnormal resin distributions (and solution mixture ratios). However, higher resin contents are often still observed near the mold faces while lower resin contents tend to prevail near the bag side and the panel

peripheries (this is common to mold-side/bag-side-type composites). For thick CCP articles receiving heat from both sides, sections near the geometrical center of the billet become the coolest regions. These areas probably lag during the cure process and consequently experience the least resin flow during final cure. These inner regions may be susceptible to some of the factors which can contribute to reduced crosslink densities. Since current CCP composites are not subject to effective post-curing operations, missing methylene links, reduced ring-to-ring bridges and dangling bonds prevail until the CCP article is heated back up during subsequent processes or during its maiden service run. Unusually high heating rates may tend to preclude the normal crosslinking process forcing these softer domains to flow out of the regional area as thermoplastics until advanced crosslinking commences.

During slow pyrolysis operations, there are typically enough meso- and macro-porous escape channels to accommodate the steady expulsion of volatiles from the local area, but this may not necessarily be the case under abnormal heating rates. It is well substantiated that phenolic-derived glassy carbons formed under pressureless charring conditions are highly porous materials. Likewise, it is well known that fully converted phenolic-matrix composites contain excessive porosity (up to 30% liquid-permeable porosity and 50% gas-permeable porosity). When as-molded phenolic composites are first pyrolyzed, they are delicate and essentially useless until matrix densification techniques are applied to build their mechanical properties back up. Additionally, pore openings and interconnectivity channels expand and widen as the temperature of the system increases. Indeed, freshly carbonized phenolic composites are so porous, they are often used to fabricate open-cell foam-type radiator cores, thermal insulators and advanced filtering substrates. The idea that the root cause of ply lifting can be attributed so heavily to internal pore pressures due to clogging effects and blockage of pore openings by a small amount of viscous liquid in the char layer is debatable . . . unless the as-molded material is so low in porosity to begin with that pore pressures begin building up before the composite article even reaches previous cure temperature levels.

This brings to mind another area of concern associated with the CCP porosity data presented earlier . . . the apparent lack of porosity exhibited in the as-molded FM5055 samples for both open and helium measured porosities. It is known that during the cure of phenolic resins, reaction volatiles create an expansive network of interconnecting, micro-porous channels leading from the interior of the phenolic matrix all the way to the outside. Additionally, it is well established that phenolic curing reactions are highly temperature-dependent, and the evidence indicates that crosslink advancement is a temperature-driven process rather than time-driven one [1]. In other words, short exposures at higher temperatures are more significant than long exposures at lower temperatures. It is during this relatively short time period, separating the gel phase from the cure phase, that the volume of flowing reaction volatiles is greatest, providing the largest pore openings, tunnel diameters and interconnecting dendrites throughout the structure.

After a few minutes at peak temperature (315°-325°F), many of the post-gel crosslinking reactions are complete while pore radii and dimensions are still significant. However, excessive time durations at temperature lead to adverse consequences. After a while, pore diameters and channel dimensions begin to shrink as the freshly solidified phenolic micro-structure continues to consolidate.

[1] There have been a number of studies over the years confirming temperature dependence over time dependency. One example includes, “Kinetics of Pyrolysis Mass Loss from MX4926 Standard Density NARC Based Carbon Phenolic Composite”, Eric Stokes, March 1994, Southern Research Institute.

If held at temperature long enough, initial gas-created micro-channels start shrinking as pore openings continue to decrease and eventually, much of pore network collapses. Gases generated after this point may inadvertently become 'trapped' volatiles. When cooled down to ambient, a composite of near-zero porosity results. Upon re-heating, existing trapped gases and newly created volatiles from the re-heating process inevitably lead to pressurized pore volumes within the material which induce the formation of micro-cracks in order to facilitate pressure releases. Phenolic materials containing at least 1% as-molded open porosity benefit to some extent by the presence of micro-cracks due to the relief of residual stresses. However, the mechanical integrity of phenolic composites with zero porosity will tend to degrade upon re-heating because the impervious hardened matrix is incapable of providing adequate pore pressure release as energy is delivered into the pore volumes.

Density and porosity characterizations have been independently conducted for A-Enka, Avtex and PAN-reinforced phenolic matrix composites cured under a multitude of experimental autoclave pressures (0 to 200psi) applied at various points throughout the cure cycle, with and without vacuum, molded to an array of maximum cure temperatures (220° to 400°F), along varying cure ramps (0.01°-10°/min) and over a variety of total cure times (3hrs-10hrs). Additionally, a variety of bagging configurations and B-staging conditions have been experimentally tested, including various types and quantities of bleeder/breather materials, custom tapered and strategically placed bleeder/breather layers, strips and ropes, a variety of solid, perorated and netted barrier films, perorated caul plates, treated release plies and special releasing concepts, peripheral damming mechanisms, modified resin formulations, pre-molded tooling aids and embedded restraint blocks, customized in-house prepreg formation, a multitude of B-staging time/temperature profiles, free-standing prepreg staging procedures vs. hot vacuum debulking, and so on (case at point: certain procedures for hot vacuum debulking have been independently shown to undermine resin distributions and composition ratios before the laminate is ever subjected to autoclave cure, yet some fabricators still practice it).

Almost every one of these parameters can adversely affect (a) localized resin content distributions and compositions throughout the article (resin-rich vs. resin-starved areas), (b) the nature and level of surface porosity and internal pore interconnectivity, (c) localized porosity distributions and the formation of pore cluster agglomerations, (d) localized fiber-resin interfacial bonding characteristics, including interphase coupling links (fiber surface-to-matrix functional group interactions), the creation and distribution of porosity sheaths and tubular voids along fiber bundle interfaces, (e) interlaminar weave meshing, crenulation interactions and ply-to-ply nesting effects, (d) composite toughness factors, and ultimately, interlaminar mechanical properties.

From these studies, it was found that both rayon and PAN based phenolic matrix composites exhibiting as-molded open porosity levels in the range 2% to 6% after autoclave cure and cool down, responded most favorably to re-heating episodes, post-cure heat treatments and pyrolysis operations with minimal micro-crack formation and with the susceptibility for pore pressure-induced delaminations virtually eliminated. Most importantly, when these laminates are re-heated back up, escape paths already exist to effectively accommodate the safe release of post-cure volatiles and pyrolysis gases. As pyrolysis commences, existing pores are etched and eroded, resulting in enlarged

pore openings and widened tunnel radii, and as the char line migrates through the material, the growing pore dimensions readily facilitate the expulsion of pyrolysis gases from the reaction layer into the highly porous char layer for safe expulsion from the system.

Ramps and holds up to and through the 180° hold were not so critical, but just before the resin begins to gel (~200°-225°F), it was found that heating ramps greater than about 4 or 5°/min often resulted in delaminations during cure or upon cool down. Additionally, hold times at peak temperature (315°-325°) which were greater than a couple of hours frequently produced delaminations when heated back up during post-cure or pyrolysis. These delaminations were attributed to the presence of abnormal residual stresses and reduced porosity leading to trapped volatiles and excessive pore pressures generated during the re-heating process. 'Residual volatiles' consist mainly of trapped water molecules and newly generated water (interstitial and hydrogen-bound water molecules shielded in regions of high crosslink density require greater than 212°F for extraction). A few percentages of trapped internal water can have profound effects on the performance and stability of the phenolic article over temperature and over its lifetime. Articles that were cured using fast ramps to the 180° hold, but very slow ramps (<< 1°/min) from the 180° hold to the 325° hold (i.e... through the gel point), with a 90 minute hold at 325° (less than 8 hours total heated autoclave time) followed by a 6 hour post-cure to 500° exhibited the greatest stability towards subsequent thermal excursions, with reduced warpage and no delams. Articles fabricated with > 100 psi cure pressure, not only exhibited low porosities, but contained an undue level of interlaminar residual stresses and frequently delaminated upon re-heat. Later on, some of the very thickest regions of certain articles begin to occasionally develop delams during pyrolysis or high temperature field use. After extensive, drawn-out investigations, residual pore pressure due to trapped volatiles in these regions was identified as the most likely culprit. Thus, extending the post-cure cycles to 24 hours and ensuring that post-cures were performed after each and every autoclave cure eliminated the delam problem permanently.

The implication is that, for high temperature applications, phenolic-based systems should be cured fairly quickly (initially) and then post-cured very slowly, maximizing the gradual and nondestructive release of residual volatiles and residual stresses before the material is ever exposed to pyrolysis temperatures. This manufacturing approach essentially conditions the phenolic composite system for optimal behavior and performance during high temperature post-processing and most importantly, during high temperature service use. Phenolic laminates which cannot survive a simple double cure, let alone an elevated post-cure, should not be used for high temperature applications[1].

There are some very close similarities between this material system (Avtex-reinforced phenolic matrix laminate) and FM5055 or MX4926, but there are also some very substantial differences between the two, particularly in terms of 'some porosity' vs 'no porosity' and heat stabilized fibers vs green fibers, as well as a vast distinction between the laminate assembly process used for each. Obviously, there is no guarantee that the trials and solutions developed for one system will work for another. The preceding history lesson was given primarily for informational purposes and hopefully to spur the imagination regarding potential solutions and ideas which might help to improve current phenolic-based composite systems whenever appropriate opportunities arise.

[1] The necessity and proven experience relating to development of an elevated temperature post-curing step for phenolic-based composites prior to pyrolysis or when the motor fires has been suggested numerous times by the author and rejected. There is an abundance of historical test data industry wide and within NASA itself more recently proving that water is released well beyond pyrolysis and throughout the burning process, not just during the factory cure cycle.

Appendix A

Basic Composite Relationships with Applications to the C-C/SiC and CCP Systems

The genesis of this system of estimation tools or so-called 'model' begin in 1982 during the author's research in carbon-carbon materials at LTV Aerospace & Defense Co. Reference the report, "*1) Relationships in Composite Fabrication and Carbon-Carbon Densification,* Randy Lee, LTV Aerospace & Defense Co., Space Shuttle Program, Leading Edge Structural Subsystem, 1982". Originally published in 1986, reformatted in 2001.

Many of the initial expressions given here can now be found in common literature sources, however, most of the subject matter dealing with composite densification processing (Appendix B) is not so easy to find. The following topics are based on concepts developed independently over several years of composites manufacturing, production and process development, particularly during an extensive series of autoclave trials and densification studies personally conducted throughout the 1980's. Over time, these principles have been optimized, refined and modified for a number of material systems including adhesives and coatings, and their applications have been documented in many publications. The version that follows has been specially adapted and formatted to apply to the material systems under study in this paper, however, most of the tools are quite applicable to all material systems, porous and non-porous.

It is mandatory that these concepts and estimation tools be based on the extensive use of subscripts, which define the particular form of the parameter in question and, when necessary, the specific processing state to which it applies. These two or three distinctions are simply separated by commas within the subscript notation scheme. While some of these designations may seem confusing at first glance, their use is intended to help clarify and define the exact parameter under discussion and hopefully, not to add confusion or make the reading process any more difficult than necessary. Also, recall that the superscript $^{-1}$ simply means 'division by' and is extensively used here to streamline an expression or laterally consolidate the equation line as a matter of personal formatting preference.

Now, it is obvious that the total weight W of a panel, billet or article is always the sum of the weights of all constituents, that is . . . $W = w_a + w_b + w_c +$ etc. . ., and the total volume of the panel, billet or article is always the sum of the volumes of all constituents . . . $V = v_a + v_b + v_c +$ etc. . . From the perspective of fractional quantities, both the sum of constituent fractions by weight and the sum of constituent fractions by volume are always unity, respectively . . . $1 = a_w + b_w + c_w + \ldots$ and . . . $1 = a_v + b_v + c_v + \ldots$ A multi-component composite system may consist of fibers, particles, aggregates, meshes, screens , binders, adhesives, surfactants, sizings, lubricants, coupling agents, etc . . .

For common binary composite systems, the weight and volume constituents may consist of a fibrous reinforcement phase f and resinous, carbon or ceramic matrix phase m. In addition, if the composite is porous and pervious to outside liquids and gases, a third volume constituent must be defined . . . the

porosity p . Thus, the basic weight, volume and fractional relationships become . . . $W = w_f + w_m$, $V = v_f + v_m + v_p$, $f_w + m_w = 1$ and $f_v + m_v + p = 1$. Note that the p fraction contributes nothing to the weight of the system and only adds internal void volume. It naturally follows that a porous composite structure requires the definition of two distinct densities in order to effectively describe the system . . . the bulk density ρ_b and the true density ρ_t , where the bulk density includes the porosity and the true density does not. Individual densities defining each of the constituents or phases are understood and straightforward . . . $\rho_f = w_f / v_f$ and $\rho_m = w_m / v_m$ for the fiber and matrix respectively (the porosity phase has no density and is a volume element only). Thus, the bulk density of the panel, billet or article can be defined as the sum of the products of each constituent density and its respective volume fraction . . .

$$\rho_b = \frac{w_f + w_m}{V} = \frac{\rho_f v_f + \rho_m v_m}{V}$$

(1A) $$\rho_b = f_v \rho_f + m_v \rho_m$$

Eq(1A) is considered (by the author) to be the master constituent relationship in which all the other expressions interconnect in some way or another as it originally formed the basis behind the development of this model. Most often, it is subjectively understood that one or more of the fractional volume constituents contains the open porosity of the composite. Since the fiber volume fraction is typically defined as an isolated constituent, it is usually surmised that the open porosity is contained within the volume of the matrix. While this approach may not always be precisely correct, it tends to help simplify most composite models. Of course this neglects any porosity which may be contained within the actual fiber bundles and individual filaments (it is well known that most fibers and tow are porous, but pore sizes may be limited to the meso and micro scale). In reality, the surface area of the pores, voids and tunnels comprising the pore network within a composite system includes a mixture of contributions from both the matrix and the fiber as well as any other constituents which may be present. For a composite system containing fiber, matrix and carbon black filler $c_{b,v}$, Eq(1A) would simply be extended to read . . .

$$\rho_b = f_v \rho_f + m_v \rho_m + c_{b,v} \rho_{cb}$$

In many of these types of composites, both the raw weight and bulk volume of the fibrous reinforcement phase remain infinitesimally constant throughout the process since they do not change chemically or physically as the substrate is subjected to the various temperatures, conditions and materials used during the densification process. Also, the total matrix phase may be the sum of several co-constituents or partial fractions in which one or more of the fractional phases change incrementally across the process. This helps to exemplify the fact that the densification process for C/C and CMC substrates is most appropriately

defined as *matrix* densification. If the matrix consists of several co-constituents, they are fully separable, and as long as the densities for each of the sub-phases is known, then . . .

$$\rho_b = f_v\rho_f + m_{v1}\rho_{m1} + m_{v2}\rho_{m2} + m_{v2}\rho_{m2} \ldots$$

Fiber and matrix volume fractions can be expressed in terms of their respective weight fractions. Since . . .

$$\rho_f = \frac{w_f}{v_f} = \frac{f_w W}{f_v V} = \frac{f_w}{f_v}\rho_b$$

. . . then . . .

(2A)
$$f_v = f_w\rho_b\rho_f^{-1} = \left(1-m_w\right)\rho_b\rho_f^{-1}$$

Likewise . . . $m_v = m_w\rho_b\rho_m^{-1}$

When the fiber volume fraction is determined early in the process, as with the C-C/SiC system, Eq(2A) can be re-written to provide estimates for the matrix content at subsequent processing states i . . .

(3A)
$$m_{w,i} = 1 - f_v\rho_f\rho_{b,i}^{-1}$$

With inclusion of the open porosity fraction, the bulk density given in Eq(1A) can be written in terms of component weight fractions. . .

$$\rho_b = \frac{W}{v_f + v_m + v_p} = \frac{W}{w_f\rho_f^{-1} + w_m\rho_m^{-1} + p_o V}$$

(4A)
$$\rho_b = \left(f_w\rho_f^{-1} + m_w\rho_m^{-1}\right)^{-1}\left(1-p_o\right)$$

The true or real composite density refers to the skeletal density which is impermeable or impervious to the particular substances infiltrated into porous substrate during processing or test characterization. While the bulk density is defined by constituent volume fractions, the skeletal or true density is a function of the weight fractions and approaches the bulk density when the open pore volume approaches zero . . .

$$\rho_t = \frac{W}{v_f + v_m} = \frac{W}{V - v_p}$$

(5A)
$$\rho_t = \rho_b\left(1-p_o\right)^{-1}$$

. . . or, as an analog to Eq(1A) and using Eq(4A), the true density can be written directly in terms of the constituent weight fractions . . .

(6A)
$$\rho_t = \left(f_w\rho_f^{-1} + m_w\rho_m^{-1}\right)^{-1}$$

Simple rearrangement of Eq(4A) can provide a couple of expressions for directly estimating open porosity from the relevant densities and the matrix content (or fiber volume) at subsequent states i . . .

(7A) $$p_{o,i} = 1-\rho_{b,i}\left[\left(1-m_{w,i}\right)\rho_f^{-1}+m_{w,i}\rho_{m,i}^{-1}\right]$$

This formula has come in handy over the years, not only in the area of advanced composites but for a variety of non-fibrous systems, including particulate coatings, adhesives and composite foams. Also, when the fiber volume fraction is determined early in the process, as done with the C-C/SiC system, Eq(4A) (or (7A)) can be re-written to provide a more convenient formula . . .

(8A) $$p_{o,i} = 1-\rho_{b,i}\rho_{m,i}^{-1}-f_v\left(1-\rho_f\rho_{m,i}^{-1}\right)$$

Of course, both Eq(7A) and (8A) can only be applied after an appropriate value for the matrix density ρ_m has been obtained, and this quantity varies according to the specific fractions defining the relevant forms of carbon, and SiC comprising the total matrix at any given state in the process, that is, ρ_m varies from state to state. For phenolic densified C/C substrates reminiscent of RCC and ACC, estimates for the matrix density at the various bimatrix and carbon states are not too difficult but for the C-C/SiC system, the procedure is more involved. Development of the distribution of partial matrix fractions across the process is provided in Appendix B and techniques for estimating the complex matrix density are given Appendix C, but first, further elaboration on process notation and subscript designation are necessary.

Physical properties and process parameters can be accompanied by a subscript representing any particular process state to which they apply. Obviously, in the dry preform state, there is no matrix so the only constituent by weight is the fibrous reinforcement fraction while the volume constituents include the fibrous fraction plus the porosity or void volume. After carbonization (pyrolysis) of the rigidization polymer, the matrix consists only of glassy carbonized polymer but after carbonization of the pitch mesophase, the matrix is comprised of both carbonized polymer plus carbonized pitch. This could be considered a 'bimatrix' state. After SMP-10 polymer resin is impregnated into the pores and pyrolyzed to 1550°F, the trimatrix composite includes: (1) carbonized polymer, plus (2) carbonized mesophase, plus (3) a-SiC ceramic. After one of the 5000° treatments, the quadmatrix may consist of: (1) carbonized polymer, plus (2) carbonized mesophase, plus (3) β-SiC ceramic, plus (4) a-SiC ceramic. Expanding on the nomenclature given in Table 3 earlier, process state descriptions and corresponding subscripts for any given property or parameter of interest can be defined appropriately as illustrated in the following diagram for the composite bulk density $\rho_{b,i}$ . . .

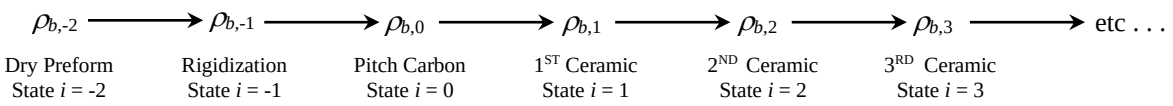

Obviously, this system is set up with the ceramic densification phase as the baseline, where the first ceramic state is designated at i = 1. This is arbitrary since the dry preform state could have been designated as i = 0, but this would undoubtedly cause confusion since the 13th PIP state would then be defined at i = 15. For some of the treatments given in this paper, the two 3000° high temp pyrolysis states can be ignored without appreciable losses in comprehension or precision. However, for estimations of the matrix density and partial matrix fractions, they cannot necessarily be omitted (as articulated in Appendix B).

In these types of systems, it is customary to obtain the weights of the articles before and after each impregnation/cure and after pyrolysis. This gives a complete picture of the weight gains and weight losses comprising each cycle of the densification process. Weights for each of the pyrolysis states can then be used to track the incremental and cumulative ceramic matrix gains from one ceramic state to the next, as well as the net ceramic weight gain overall. Raw weights for the pyrolyzed articles (or rather raw bulk density measurements in our case) will permit estimations of the intermediate carbon gains, the incremental and cumulative ceramic weight gains, the intermediate carbon matrix contents, and the incremental and cumulative ceramic matrix contents. This will allow a comprehensive quantification of the total matrix fractions and each of the contributing partial fractions across the entire densification process.

Appendix B

Estimation of Total and Partial Matrix Weight Fractions for the C-C/SiC System

At the state i = -2 , the composite consists only of dry fiber preform in which the matrix fraction is zero. But after rigidization via polymer impregnation, cure and pyrolysis to the state i = -1, a small amount of glassy carbon is deposited which permanently becomes part of the inorganic carbonaceous fraction of the total matrix. If W_{-2} is the raw weight of the dry preform before rigidization (after weaving) and W_{-1} is the raw weight of the rigidized preform after pyrolysis, the fractional weight gain going from the state i = -2 to the state i = -1 can be defined as the latter minus the former divided by the former, that is . . .

$$\eta_{-2\rightarrow -1} \;=\; \frac{W_{-1}-W_{-2}}{W_{-2}} \;=\; \frac{\left(w_f + w_{cp}\right)-w_f}{w_f} \;=\; \frac{w_{cp}}{w_f}$$

where w_{cp} is the raw weight of the carbonized rigidization polymer fraction (and w_f is the raw weight of fiber). Since the raw volume of the substrate is considered to be constant throughout the densification process, this can be written in terms of the reported bulk densities respectively, that is . . .

$$\eta_{-2\rightarrow -1} \;=\; \frac{\rho_{b,-1} - \rho_{b,-2}}{\rho_{b,-2}}$$

Chances are, since the substrate volume is invariant (or only changes infinitesimally), FMI probably obtains the raw volume of the preform at the very beginning of the process (to derive the constant fiber volume reported earlier) and then simply weighs the articles before and after thus avoiding having to make tedious volumetric measurements on the article(s) after each and every cycle.

Now the total matrix content at the state i = -1 (which consist only of carbonized rigidization polymer at this point), is defined as . . .

$$m_{w,-1} \;=\; \frac{w_{cp}}{w_f + w_{cp}} \;=\; \left(1 \;+\; \frac{w_f}{w_{cp}}\right)^{-1}$$

. . . and using the definition for $\eta_{-2\rightarrow -1}$ given above, the total matrix content at i = -1 can be written in terms of the FMI-measured bulk densities for the substrate . . .

(1B) $$m_{w,-1} \;=\; \left[1 \;+\; \rho_{b,-2}\left(\rho_{b,-1} - \rho_{b,-2}\right)^{-1}\right]^{-1}$$

Next, after impregnation and pyrolytic conversion of the pitch resin into carbonized pitch mesophase, that is, at i = 0, the total matrix fraction consists of two partial fractions . . . the carbonized rigidization polymer fraction $\partial_{cp} m_{w,0}$ deposited during the first cycle from state i = -2 to i = -1 and the carbonized pitch mesophase fraction $\partial_{cm} m_{w,0}$ deposited during the second cycle as the substrate is carried from i = -1 to

i = 0 in accordance with total matrix fraction at i = 0 . . . $m_{w,0} = \partial_{cp} m_{w,0} + \partial_{cm} m_{w,0}$. Independent definition and rearrangement of these two partial matrix fractions follow . . .

$$\partial_{cp} m_{w,0} = \frac{w_{cp}}{W_0} = \frac{w_{cp}}{w_f + w_{cp} + w_{cm}} = \left(1 + \frac{w_f + w_{cm}}{w_{cp}}\right)^{-1}$$

and . . .

(2B) $$\partial_{cm} m_{w,0} = \frac{w_{cm}}{W_0} = \frac{w_{cm}}{w_f + w_{cp} + w_{cm}} = \left(1 + \frac{w_f + w_{cp}}{w_{cm}}\right)^{-1}$$

where the subscripts cp and cm represent carbonized rigidization polymer and carbonized pitch mesophase respectively. Now the *incremental* weight gain from the state i = -1 to i = 0 concerns the partial fraction of carbonized mesophase deposited in the pores and is defined as . . .

(3B) $$\eta_{-1\to 0} = \frac{W_0 - W_{-1}}{W_{-1}} = \frac{\rho_{b,0} - \rho_{b,-1}}{\rho_{b,-1}} = \frac{w_{cm}}{w_f + w_{cp}}$$

. . . while the *cumulative* weight gain from the state i = -2 to i = 0 encompasses the total matrix fraction from the beginning of the process to the current state of interest . . .

(4B) $$\eta_{-2\to 0} = \frac{W_0 - W_{-2}}{W_{-2}} = \frac{\rho_{b,0} - \rho_{b,-2}}{\rho_{b,-2}} = \frac{w_{cp} + w_{cm}}{w_f}$$

In analogy to Eq(1B), use of the cumulative weight gain Eq(4B) permits the estimation of the total matrix content at the state i = 0 simply by knowing the FMI-measured bulk densities for the substrate . . .

$$m_{w,0} = \frac{w_{m,0}}{W_0} = \frac{w_{cp} + w_{cm}}{w_f + w_{cp} + w_{cm}} = \left(1 + \frac{w_f}{w_{cp} + w_{cm}}\right)^{-1}$$

$$m_{w,0} = \left[1 + \rho_{b,-2}\left(\rho_{b,0} - \rho_{b,-2}\right)^{-1}\right]^{-1}$$

Similarly, Eq(2B) and the incremental weight gain Eq(3B) permit estimation of the partial matrix fraction resulting from the carbonized pitch mesophase contribution at the state i = 0 . . .

$$\partial_{cm} m_{w,0} = \left[1 + \rho_{b,-1}\left(\rho_{b,0} - \rho_{b,-1}\right)^{-1}\right]^{-1}$$

. . . and the corresponding partial fraction representing the carbonized rigidization polymer at i = 0 can be deduced by difference . . . $\partial_{cp} m_{w,0} = m_{w,0} - \partial_{cm} m_{w,0}$.

The 'partial' symbol used here bears no operational relationship to partial differentiation; it is utilized here in a symbolic fashion.

The first true ceramic cycle in the process from the state $i = 0$ to $i = 1$ deposits a-SiC into the pores of the C/C substrate, and the total matrix consists of three partial fractions . . . $m_{w,1} = \partial_{cp} m_{w,1} + \partial_{cm} m_{w,1} + \partial_{S1} m_{w,1}$, where the subscript $S1$ represents the first SiC fractional deposit in the process. Using the same procedure demonstrated above, the incremental and cumulative (ceramic) weight gains can be defined so that the total matrix fraction and the partial (SiC) matrix fraction are given in terms of the measured substrate bulk densities. Respectively . . .

$$m_{w,1} = \left[1 + \rho_{b,-2}\left(\rho_{b,1} - \rho_{b,-2}\right)^{-1}\right]^{-1} \qquad \text{and} \qquad \partial_{S1} m_{w,1} = \left[1 + \rho_{b,0}\left(\rho_{b,1} - \rho_{b,0}\right)^{-1}\right]^{-1}$$

. . . or in general, at any future state of interest i . . .

(5B) $$m_{w,i} = \left[1 + \rho_{b,-2}\left(\rho_{b,i} - \rho_{b,-2}\right)^{-1}\right]^{-1}$$ Cumulative (Total) Matrix Content

. . . and

(6B) $$\partial_{S1} m_{w,i} = \left[1 + \rho_{b,(i-1)}\left(\rho_{b,i} - \rho_{b,(i-1)}\right)^{-1}\right]^{-1}$$ Incremental (Fractional) Matrix Content

Hence, similar to Eq(3A) given in Appendix A, the total matrix content at any state in the process can be estimated from a single measured parameter, namely, the composite bulk density at the same state (formulas (3A) and (5B) produce the same exact results since the coefficients used in both are derived from the same constants or invariants). Formula (6B) above, which estimates the incremental or cycle-to-cycle weight gain, is the primary tool for constructing a comprehensive table quantitatively reflecting the distribution of partial matrix fractions in the C-C/SiC system for the four matrix co-constituents as they evolve across the densification process.

First however, recall that after the 5th and 10th densification cycles (at $i = 5$ and $i = 10$), a 3000° heat treatment (HT) is applied which converts all the a-SiC into β-SiC. This results in a reduction of the bulk matrix volume along with an accompanying change in the nature and quantity of open and closed porosity within the matrix phase . . . but the matrix weight fraction remains infinitesimally unchanged (the transition from $\text{a-SiC} \rightarrow \beta\text{-SiC}$ does not result in degradation or volatile release since it only involves a microstructural transition process; and the two carbon forms are thermally inert at this temperature). During earlier evaluations, these two points were subdued in order to simplify the analysis and because their effects are considered to be insignificant relative to the overall average properties which are being examined. For this analysis however, illustration of these two heat treatments could be enlightening. Using formulas (5B) and (6B) as the primary data generators, Table 1B below was constructed which depicts the

distribution of the four matrix co-constituents across the entire densification process: carbonized rigidization polymer (glassy carbon), carbonized pitch mesophase, glassy a-SiC and crystalline β-SiC. This is provided in the upper sub-table. The lower sub-table consolidates the two carbon forms and the two SiC forms to reflect a simplified 'bimatrix' system. The sum of either sub-table equals the total matrix content.

Table 1B. Process distribution of partial matrix fractions for the C-C/SiC composite system.

Quadmatrix

PIP Cycle	-1	0	1	2	3	4	5	3000°HT	6	7	8	9	10	3000°HT	11	12	13
Glassy C	16.0%	13.6%	12.4%	11.2%	10.1%	9.0%	8.7% →	8.7%	8.4%	8.2%	8.1%	7.9%	8.0% →	8.0%	7.8%	7.7%	7.5%
Pitch C		15.0%	13.7%	12.4%	11.2%	10.0%	9.6% →	9.6%	9.3%	9.0%	8.9%	8.8%	8.9% →	8.9%	8.7%	8.5%	8.3%
a-SiC			8.8%	15.9%	21.8%	26.9%	28.7% ↘		2.9%	5.7%	6.9%	8.1%	7.3% ↘		2.6%	4.5%	6.2%
β-SiC								28.7%	27.9%	27.0%	26.7%	26.3%	26.5% →	33.8%	33.0%	32.3%	31.7%

Bimatrix

Total C	16.0%	28.6%	26.1%	23.6%	21.3%	19.1%	18.3% →	18.3%	17.8%	17.2%	17.0%	16.7%	16.9% →	16.9%	16.5%	16.1%	15.8%
Total SiC			8.8%	15.9%	21.8%	26.9%	28.7% →	28.7%	30.7%	32.7%	33.5%	34.4%	33.8% →	33.8%	35.5%	36.8%	37.9%

Total Matrix

Sum	16.0%	28.6%	34.9%	39.5%	43.1%	46.0%	47.0% →	47.0%	48.5%	50.0%	50.5%	51.1%	50.7% →	50.7%	52.0%	52.9%	53.8%

This analysis indicates that when the FMI densification process is complete, that is, after PIP#13 (at i = 13), the matrix consists of about 16% total carbon and about 38% total SiC. As expected, the SiC phase is overwhelmingly dominated by β-SiC while the ~ 6% a-SiC fraction is all located within the periphery of the material. Graphical plots of the partial matrix fractions and the consolidated bimatrix data are given in Figure 1B below. As the data illustrates, a-SiC disappears during each 3000° HT being replaced with β-SiC as the a-SiC level incrementally recovers (to a lesser degree). Of course, this presumes that 100% of the a-SiC present in the system is completely transformed into β-SiC when the 3000° HT is applied. While this may be debatable to some, there is no reason at this point to believe otherwise.

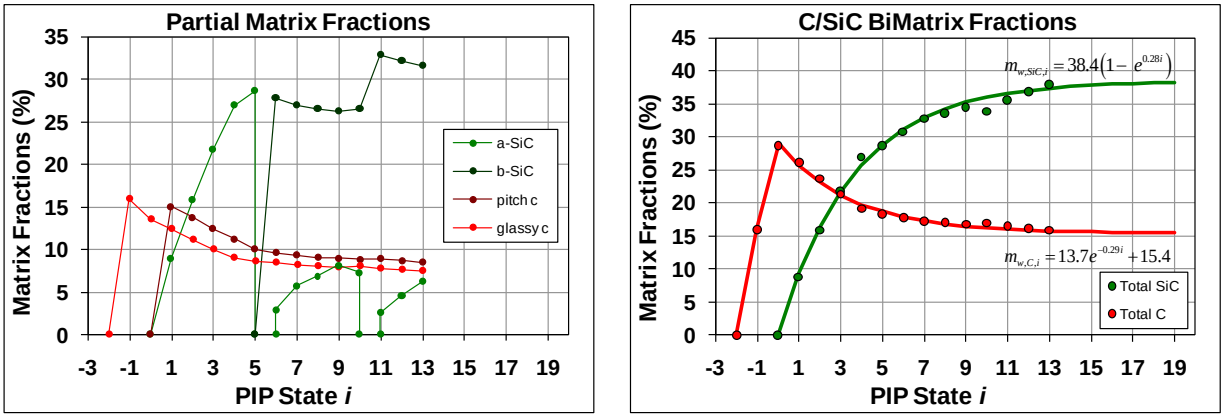

Figure 1B. Data plots and representative curves for the Quadmatrix and Bimatrix values given in Table 1B.

As the net carbon content gradually decreases over the process, the ceramic fraction incrementally fills up the matrix porosity. Analytically, it is indicated that the maximum SiC content at infinite densification (if that were possible) will be less than 40%. These fractional matrix quantities can be used to pursue other properties, such as the complex matrix density.

Appendix C

Estimation of Complex Composite Matrix Densities for the C-C/SiC System

It is extremely difficult to physically measure the density of multi-fractional matrices within most composite systems, particularly carbon and ceramic matrix systems. More importantly, it is physically impossible to directly ascertain the matrix density in the C-C/SiC system which changes from state-to-state. Thus, astute estimation methods must be employed, and even these approaches are difficult to accurately execute with any appreciable degree of confidence that the results will be meaningful and realistic. However, with the information that is now at hand, this task becomes quite feasible. The potential value associated with this type of analysis can provide a unique and critical piece of the puzzle needed to effectively characterize and quantify specialized material properties which can often only be speculated on.

During the early process stages, the C-C/SiC matrix consists only of inorganic carbon. By the end of the densification process, the matrix contains four co-constituents or partial fractions in which each has its own unique bulk and true density. However, in accordance with the principles set forth by the fundamental composite relationships implied in Eq(1A) and (5A), these complex matrix densities can be reasonably estimated if the fractional weight coefficients for each constituent are known to a reasonably accurate degree. Relevant fractional quantities were determined in Appendix B. Now, if the open porosity fraction in Eq(5A) is taken to zero, the resulting net density becomes a representative function of the particular densities utilized for the co-constituents. For instance, the use of co-constituent bulk densities (that is, liquid-permeable densities), provides an expression for estimating the net bulk (liquid-permeable) density of the complex matrix, that is . . .

(1C) $$\rho_{m,i} = \left(c_{p,i}\, \rho_{cp}^{-1} + c_{m,i}\, \rho_{cm}^{-1} + s_{a,i}\, \rho_{a\text{-}SiC}^{-1} + s_{\beta,i}\, \rho_{\beta\text{-}SiC}^{-1} \right)^{-1}$$

where $c_{p,i}$, $c_{m,i}$, $s_{a,i}$ and $s_{\beta,i}$ are the fractional weight coefficients for carbonized rigidization polymer, carbonized pitch mesophase, amorphous (glassy) SiC and crystalline SiC respectively at any state of interest i, along with their corresponding bulk densities (as provided in Table 1 near the beginning of the report), namely, $\rho_{cp} \simeq$ 1.45 g/cc, $\rho_{cm} \simeq$ 1.35 g/cc, $\rho_{a\text{-}SiC} \simeq 2.45$ g/cc and $\rho_{\beta\text{-}SiC} \simeq 2.95$ g/c , which are considered to be the effective densities relevant to all liquid impregnations, intrusions and infiltrations.

Table 1C below provides estimates for the net matrix bulk density across the densification process based on the previously determined partial matrix fractions and the corresponding co-constituent matrix bulk density averages from Table 1. This is followed by a graphical plot of these results in Figure 1C.

Table 1C. Net matrix bulk density estimated from partial matrix weight fractions and co-constituent matrix bulk densities.

Process State *i*	-1	0	1	2	3	4	5	3000°HT	6	7	8	9	10	3000°HT	11	12	13
Matrix Bulk Density (g/cc)	1.45	1.40	1.57	1.69	1.78	1.87	1.89	2.06	2.08	2.10	2.10	2.11	2.11	2.15	2.16	2.17	2.18

Figure 1C. Graphical depiction of the bulk matrix density for the C-C/SiC system as it changes across the densification process.

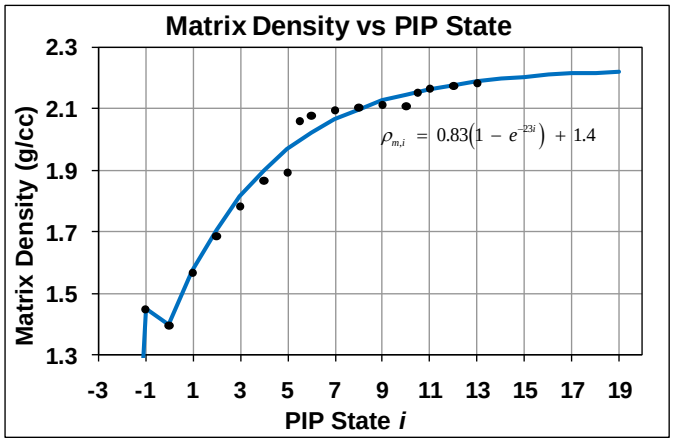

While this data does not exactly lend itself to accurate or meaningful curve modeling, there is an indication that the maximum bulk matrix density tends to approach ~ 2.23 g.cc after infinite densification. Now, this is the matrix density under the scenario or pretense that the open composite porosity fraction is completely contained within the matrix volume. Obviously, this is slightly over-simplistic but the approach has demonstrated valid results for a number of composite systems. From another perspective, net bulk matrix densities would be even lower if some of the *closed* porosity fraction was also sealed within the matrix. For example, the true (liquid-impervious) matrix volume at the state i = 13 is around ~43% but with inclusion of the ~13% average open composite porosity, the bulk matrix volume comes closer to ~56%. However, this is a misnomer since the ~13% porosity is open. If absolute densities for each of the matrix constituents were considered (that is, 2.26 for carbon and 3.21 for SiC) resulting in a total porosity of about ~23%, the net matrix bulk density would be substantially lower. In any case, the liquid impervious matrix volume is still ~43% and the true matrix density remains unchanged regardless. Open and closed porosity may sometimes seem like a world apart in terms of accessibility and permeability but geographically, these pores may only be separated by a few angstroms across a thin wall of matrix material which just happens to be stout, impervious and isolated from the immediate local surroundings.

Appendix D

Estimation of Densities for Hypothetical Cases in the C-C/SiC System

It is interesting to speculate on what the final substrate density might be if the material were completely densified with carbonized pitch matrix throughout, or if it were densified exclusively with β-SiC, or . . . if the ~13.4% remnant porosity characteristic of the fully densified substrate at i = 13 were somehow completely filled with one of these matrix materials. Speculation densities for this system are not difficult to estimate given all the other information that is now available. First however, briefly examine how each constituent changes as the substrate is processed through the succession of densification cycles by re-evaluating the development of Eq(1A) and Eq(4A) given in Appendix A. Using the symbols . . . ↑ to designate an 'increasing' variable; ↓ for 'decreasing'; and — for 'no change', it can be visualized how the bulk density of the substrate increases only because specific constituents increase while other constituents either decrease less or do not change at all. Consider the concerted forms of Eq(1A) and Eq(4A) . . .

↑ ↑ — ↑ — — ↑ ↑ ↓ — ↑ ↑ ↓

$$\rho_b = \frac{W}{V} = \frac{w_f + w_m}{v_f + v_m + v_p} = f_v\rho_f + m_v\rho_m = \left(f_w\rho_f^{-1} + m_w\rho_m^{-1}\right)^{-1}(1-p)$$

— — ↑ ↓

Volume Fractions *Weight Fractions*

Not surprisingly, the raw matrix volume increases at the expense of the porosity volume while the total (raw) volume of the article or panel remains constant. This is also reflected in the fractional expressions.

Now, consider the increase in bulk density due to an incremental weight quantity w_x introduced into the remnant pores of the substrate above and beyond the matrix weight which is already present w_m, that is . . .

— — ↑ — — ↑ — — — ↑

$$\rho_b = \frac{w_f + w_m + w_x}{V} = \frac{w_f + w_m}{V} + \frac{v_x\rho_x}{V} = \frac{w_f + w_m}{V} + \rho_x x_v$$

. . . and so the change in the bulk density is due only to weight contributed by the partial volume fraction of the new material x_v as it occupies the existing pore volume, as given simply by . . .

$$d\rho_b = \rho_x d x_v$$

In general, the bulk density at any future state ρ_b can be estimated simply by appending the bulk density at a previous state $\rho_{b,o}$ with the density contribution from the new material $x_v\rho_x$, that is . . .

(1D) $$\rho_b = \rho_{b,o} + x_v\rho_x$$

where ρ_x is the density of the new material and x_v is the volume fraction of the same. For the purposes intended here, x_v might represent the former open porosity now occupied by the new material, or at least, a portion of the open porosity . . . since the porosity asymptotically approaches a minimum limit or threshold, even after many densification cycles, it is physically impossible to attain zero porosity with these types of material systems. Consider the following examples. It has now been inferred that the threshold porosity for the FMI C-C/SiC system approaches ~12%, while threshold porosities for 2-D laminated and 3-D braided phenolic-densified C/C forms have been independently confirmed to approach ~3% and ~8% respectively.

Threshold porosity p_t can also be considered as unavailable porosity due to the constrictions of the material system being densified. Thus, it can be accounted for in Eq(1D) simply by modifying the pore volume available to the densifying material, that is . . .

(2D) $$\rho_b = \rho_{b,o} + \left(x_v - p_t\right)\rho_x$$

For the sake of curiosity, consider first situations in which the remaining 13% porosity in the C-C/SiC substrate were carried to full theoretical density, being densified say with β-SiC, or carbonized pitch or pyrolytic carbon. This act would constitute a 14th densification cycle carrying the substrate to the i = 14 state. While it is physically impossible to attain zero porosity with PIP-type (liquid-densified) substrates, including essentially all C/C and CMC forms, it is interesting to wonder what the final density might be if all the residual porosity at the state i = 13 were fully saturated with β-SiC or carbonized pitch.

Evidence for the C-C/SiC system under study indicates that the average threshold open porosity is very close to 13% for liquid densification using SMP-10 carbosilane resin low fired to the a-SiC state. Phenolic/furfurylol liquid-densified systems such RCC and ACC have been proven to exhibit a threshold porosity of about ~3%, which is probably comparable to pitch-densified approaches as well. However, it has been shown that the fraction of closed porosity increases with excessive liquid-densification cycles, and the formation of closed porosity has also been demonstrated during CVD/CVI densifications when the process parameters are not fully optimized. Using Eq(2D), various scenarios can be estimated as given in the table below and further elaborated on in Tables 7 and 8 on pages 18 and 19 in the report.

Glassy Carbon[1] ρ_b = 1.45	Pitch Carbon[2] ρ_b = 1.35	a-SiC ρ_b = 2.45	β-SiC ρ_b = 2.95	β-SiC ρ_b = 3.21	Kerosene $\rho_b = 0.817^{77°F}$	Water $\rho_b = 0.998^{77°F}$	Phenolic Resin[3] ρ_b = 1.24
1.94 g/cc	1.92 g/cc	2.07 g/cc	2.14 g/cc	2.17 g/cc	1.85 g/cc	1.88 g/cc	1.91 g/cc

Appendix E

Conversion Ratios & Interpretation of Pyrolysis Weight Losses for the CCP System

As with all the preceding Appendices, it is recommended that the topics introduced in Appendix A, particularly the specific subscript nomenclature formulated there, be understood in order to fully appreciate the ideas developed here and throughout the report.

It is well known, the first derivative of a function gives the slope of that function, typically providing another function which represents the instantaneous rate or ratio of the dependent variable to the independent variable. Setting this first derivative to zero provides a method to evaluate the relative maxima and minima of the function. Similarly, the second derivative gives a functional method for evaluating the extreme points pertaining to the first derivative function, namely, the inflection points which are often located mid way between the first derivative extreme points. For the trigonometric functions defining models in the CCP analysis, these derivatives are classical and straightforward . . .

(1E) $$\frac{d}{dx}a\left[1\pm ArcTan\left(-bx+c\right)+d\right] \;=\; \pm\frac{ab}{1+\left(c-bx\right)^2}$$

The derivative of the first derivative or the second derivative of the primary function gives . . .

$$\frac{d^2}{dx^2}a\left[1\pm ArcTan\left(-bx+c\right)+d\right] \;=\; \pm\frac{2ab^2\left(c-bx\right)}{\left(1+\left(c-bx\right)^2\right)^2}$$

The value of x at all the points where this second derivative is equal to zero represents the inflection points (the transitional points separating increasing and decreasing regions along the original curve). There is only one inflection point along the regions of interest in these functions and is found to simply be . . .

(2E) $$x \;=\; \frac{c}{b}$$

In analogy to the weight gain relationships developed in Appendix B, the fractional *weight loss* that a freshly fabricated panel or article in the as-molded state A of raw weight W_A experiences as it undergoes pyrolysis to the first carbon state 0 defined by the raw weight W_0 is given as the former weight minus the latter weight divided by the former, that is . . .

$$\eta_{A\to 0} \;=\; \frac{W_A-W_0}{W_A} \;=\; \frac{\left(w_f+w_{cb}+w_r\right)-\left(w_f+w_{cb}+w_{cp}\right)}{W_A} \;=\; \frac{\left(w_r-w_{cp}\right)}{W_A}$$

where w_f, w_{cb}, w_r and w_{cp} are respectively, the raw weights of the fibrous reinforcement, the carbon black particles, the virgin cured phenolic resin and the carbonized (glassy) phenolic resin char. Recall that the ultimate or threshold char yield y_t after 100% conversion of cured phenolic resin samples is a constant and has been previously substantiated to be[1] . . . $y_t = w_{cp}/w_r = 56.0\%$. Then the fractional pyrolysis weight loss from the state A to the state 0 becomes . . .

$$\eta_{l,A\to 0} = \frac{w_r - w_{cp}}{W_A} = \frac{w_r - y_t w_r}{W_A}$$

(3E) $$\eta_{l,A\to 0} = r_w\left(1 - y_t\right)$$

. . . which gives a method for estimating the resin content r_w by measuring the pyrolysis weight loss of the article (that is, as long as a reliable average value for y_t is maintained).

Now, at any point during the pyrolysis process, the instantaneous char yield y can be defined as the ratio of the converted resin weight w'_{cp} to the original resin weight, that is . . . $y = w'_{cp}/w_r$, which goes to y_t as $w'_{cp} \to w_{cp}$. Also, the normalized char yield Y can be defined accordingly . . . $Y = y/y_t$. By this definition, Y can be specifically identified as the extent of pyrolysis or *degree of conversion* of virgin resin to carbon char. Now, at any point during the conversion (pyrolysis) process, the total weight of matrix consists of converted resin $w'_{cp} = yw_r$, and unconverted resin $w'_r = \left(1-Y\right)w_r$ so that the instantaneous fractional weight loss η_l at any time during pyrolysis becomes . . .

$$\eta_l = \frac{w_r - \left(w'_r + w'_{cp}\right)}{W_A} = \frac{w_r Y\left(1 - y_t\right)}{W_A}$$

. . . and the degree of pyrolytic conversion reduces to . . .

(4E) $$Y = \frac{\eta_l}{r_w\left(1 - y_t\right)}$$

which expresses the degree of conversion in terms of the partial pyrolysis weight loss physically measured at any chosen point during the charring process.

[1] Reference item number 4 on page 31.

All analytical and technical descriptions as well as illustrations throughout this paper are the interpretation and handiwork of the author except where noted.